

A Comprehensive Analysis of Fermi Gamma-Ray Burst Data with thermal and non-thermal component

ABSTRACT

Aims: We have investigated the properties of thermal and non-thermal components as well as the effect of the thermal components on the overall gamma-ray burst (GRB) spectra with 20 GRBs observed by Fermi/GBM.

Methodology: We first comprehensively compare the fitting results of the two different models (Band Only and Band+Blackbody (BB)) in the time-resolved spectra. We then use Compton function + Blackbody+ power law (CPL+BB+PL) model to fit the time-resolved spectra. Finally, we present the spectral evolutions between the spectral parameters and their physical significance.

Results: The thermal component decrease the low-energy index α and does not seem to affect high-energy index β ; the thermal component makes the peak energy E_p increase and it leads to faster decay of E_p in decaying episodes. Four GRBs can be fitted by the model, which shows that PL component appears in the energy spectrum at the beginning of the fireball explosion.

Conclusion: (i) there are a little bursts satisfied with the synchrotron radiation through the analysis of the low-energy power-law index α ; (ii) although the jitter radiation can explain the evolutions of α for three bursts, the possibility of the occurrence is too low; (iii) comparing the particle acceleration models in GRBs, the magnetic reconnection is more suitable to the prompt emission than the internal shock; (IV) the correlation between spectral peak energy E_p and thermal temperature kT shows that there are magnetically-dominant jets in the GRBs; (V) the E_p - F_p relation is weak in Band+BB, which may be regarded as one of the evidences of the existence of the thermal radiation in GRB prompt emission.

Keywords: Gamma-ray bursts: general – methods: statistical – radiation mechanisms: thermal components non-thermal components

1. INTRODUCTION

Gamma-ray bursts (GRBs) are the most energetic explosions at cosmological distances (Meegan et al. 1992; Bhat & Guiriec 2011). It is most likely caused by the result of cataclysmic events such as the collapse of a massive star (Woosley 1993; MacFadyen & Woosley 1999) or the merger of two dense objects (Paczynski 1986; Fryer et al. 1999; Rosswog 2003). Though various observations and theory studies have been carried out over 50 years after the discovery of the GRB, there are still many unresolved problems in the prompt emission phase. The prompt emission mechanism of GRBs is one of the unresolved issues. Regardless of the nature and formation mechanism of the GRB central engine, the fireball model is still the most popular theoretical model in GRBs. Internal-external-shock model can explain the prompt emission and afterglow based on the fireball model. (Tavani 1996; Zhang & Mészáros 2004; Mészáros and Rees 1993; 1997; Sari et al. 1998). Some evidences showed Poynting-flux-dominated outflow model could provide a viable mechanism for generating the observed prompt emission (e.g., Giannios 2009; Zhang & Yan 2011). Moreover, the fireball model also predicts strong thermal emission emanating from the jet's photosphere (Paczynski 1986; Goodman 1986; Zhang 2014).

Analysis of the prompt emission spectroscopy can provide us valuable clues to understand prompt emission mechanism. The empirical Band function (Band et al. 1993), has traditionally been fitted to provide a good description of the prompt emission spectra. However, many studies revealed that the single Band function cannot well interpret the spectra of entire GRBs. For example, Ryde et al. (2014) showed the spectra is thermal (blackbody (BB)) at the beginning and later become non-thermal. Since then, many studies showed that GRB spectra are composed of two components, thermal and non-thermal component even three components. These components can be BB, Band or a power-law with an exponential cutoff (hereafter CPL). In addition, there may be a power-law component in some GRBs (e.g. Ackermann et al. 2010; Guiriec et al. 2011, 2013, 2015a, 2015b; Ryde 2005; Pe'er & Ryde 2009).

Spectral evolution of GRBs is a common phenomenon. The peak energy E_p of νF_ν spectra decays with time, $E_p \propto t^{-\delta}$, during the decay pulse (Crider et al. 1997; Daigne & Mochkovitch 2003; Peng et al. 2009). In addition, the thermal energy kT of BB spectra also decay with time following almost the same δ (Pe'er 2008; Ryde & Pe'er 2009). Previous studies have shown that E_p is positively correlated with low-energy power-law index α , $E_p \propto T^\alpha$, (Burgess et al. 2014a) and the same correlation $kT \propto t^{-\alpha}$ also exist (Pe'er 2008; Ryde & Pe'er 2009).

Some studies analyzed some single burst including a significant thermal spectral contribution to check the effects of the thermal components on the non-thermal components as well as hardness-luminosity relation (Guiriec et al. 2011, 2013, 2015a, 2015b). For example, Huang et al. (2016) perform a detail analysis of the spectra of GRB100724B which is dominated by the empirical Band function form, includes a significant thermal spectral contribution (Guiriec et al. 2011). However, they focus their attentions on the single burst. In this paper we would like to comprehensively study 20 bursts with thermal and non-thermal components to investigate how the thermal component simultaneously may affect the non-thermal component, the whole shape and evolution of the spectra, and we compare our results with previous studies. In section 2 we describe the Fermi GBM observations and the analysis methods. We present our fitting results in section 3 and section 4. Discussion and conclusions are given in section 5. We have adopted the cosmological constant $H_0 = 70 \text{ km s}^{-1} \text{ Mpc}^{-1}$, $\Omega_m = 0.3$.

2. THE SAMPLE SELECTION AND DATA ANALYSIS

The Fermi satellite was launched in 2008 which is composed of Gamma-ray Burst Monitor and Large Areas Telescope. To study the spectral components and evolutions from keV to MeV Band, we select the GRB data detected by Fermi GBM from 1 January 2012 to 1 July 2016 in FSSC (Fermi Science Support Center), which converge an energy range from 8 keV to 40 MeV (Meegan et al. 2009). We adopt the TTE file, which is one of the GBM spectral files and has the finest time (2 μs) and energy evolution, for the purpose of the time-resolved analysis in the prompt emission spectra. In the other hand, the burst which we selected should be bright and sufficiently high signal-to-noise. Therefore, these bright bursts satisfy criteria which are same to Yu et al. (2016) as follows: the energy flux $F_\nu \geq 4 \times 10^{-5} \text{ erg s}^{-1} \text{ cm}^{-2}$ and the peak photon flux $F_p \geq 20 \text{ photos s}^{-1} \text{ cm}^{-2}$. We excluded some bursts that the T_{90} is more than 300 s because the TTE data are available from 30 s before triggers to 300 s after triggers. There are 67 bursts meet the criteria.

For each burst, we selected detectors of NaI detectors and BGO according to the quicklook.pdf photo and presented that in Table 1. Besides, the energy range of NaI and BGO is from 8 keV to 900 keV and from 250 keV to 40 MeV, respectively. Moreover, it is necessary to perform the background fitting before the spectral analysis, and the background was fitted with a polynomial function with order 2-4 through two background-intervals, before and after the emission pulses. The data was fitted by Rmfit 4.3.2 package and the minimizing statistics in the fitting is the Castor C-Statistics (Cash 1979, hereafter C-

stat), which is a likelihood technique converging to a χ^2 for a specific data set when there are enough counts (Guiriec et al. 2015b).

Table 1 The sample bursts with their duration and detector

GRB	T90 / s	NaI	BGO
100724029	114.690	n1 n2 n5	b0
120129580	3.072	n7 n8 nb	b1
120707800	40.960	n6 n9 nb	b1
121225417	58.497	n1 n3 n5	b0
130305486	25.600	n6 n9 na	b1
130502327	24.320	n6 n7 n8	b1
130504978	73.217	n6 n9 na	b1
130518580	48.577	n0 n3 n4	b0
130606497	52.225	n7 n8 n11	b1
131231198	31.232	n0 n3 n4	b0
140206275	146.690	n0 n1 n3	b0
140329295	21.504	n7 n8 nb	b1
140523129	19.200	n0 n3 n4	b0
150201574	15.616	n0 n3 n4	b0
150314205	10.688	n9 na	b1
150403913	22.272	n3 n4	b0
150627183	64.577	n3 n4	b0
150902733	13.568	n0 n1 n3	b0
151227218	43.008	n1 n2 n5	b0
151231443	71.425	n8 nb	b1
160422499	12.288	n0 n1 n3	b0

Table 2 Time-integral spectrum fitting results for 20 bursts

GRB	model	Band/CPL			BB	CPL/PL		$F_p / \text{keV s}^{-1} \text{cm}^{-2}$	C-stat/DOF
		$E_{\text{peak}}/\text{keV}$	α	β	kT/keV	$E_{\text{peak}}/\text{keV}$	p		
120129580	Band	276.8±6.81	-0.75±0.02	-2.46±0.06				6.75e-6±4.80e-8	853/481
	Band+BB	290.6±8.90	-0.62±0.04	-2.54±0.08	11.41±0.65			6.79e-6±5.00e-8	789/479
	Band+PL	291.6±9.34	-0.78±0.05	-2.52±0.13			-1.73	6.82e-6±2.70e-7	857/479
	CPL+BB+PL	366.0±13.80	-0.81±0.06		18.73±1.21		-1.36±1.85	6.97e-6±6.20e-8	815/478
120707800	Band	123.60±6.54	-0.89±0.05	-2.12±0.03				1.42e-6±1.30e-8	1492/360
	Band+BB	132.50±9.72	-0.47±0.23	-2.15±0.03	7.76±0.55			1.41e-6±1.30e-8	1467/358
	Band+PL	141.00±6.93	-0.98±0.04	-2.26±0.05			0.09±0.51	1.38e-6±1.60e-8	1449/358
121225417	Band	307.40±15.20	-1.15±0.01	-2.13±0.62				8.50e-7±8.40e-9	911/504
	Band+BB	667.10±99.80	-1.36±0.03	-2.43±0.22	32.69±1.42			8.73e-7±1.10e-8	876/502
	Band+PL	242.40±21.70	-0.88±0.23	-2.05±0.05			-0.98±1.25	8.41e-7±8.20e-9	888/502
	CPL+BB+PL	707.7±104.00	-1.37±0.02		38.53±4.73			8.76e-7±9.90e-9	870/501
130502327	Band	286.20±4.45	-0.60±0.01	-2.45±0.05				2.76e-6±1.70e-8	1001/483
	Band+BB	333.90±13.00	-0.68±0.02	-2.62±0.08	27.67±2.21			2.76e-6±1.70e-8	983/481
	CPL+PL	310.3±5.87	-0.63±0.03				-1.25±0.18	2.71e-6±1.80e-8	1098/482
	CPL+BB+PL	378.00±12.50	-0.74±0.03		29.88±1.42		-1.21±0.38	2.79e-6±2.80e-8	1008/480
130305486	Band	549.40±20.70	-0.51±0.02	-2.28±0.08				1.74e-6±2.10e-8	1060/501
	Band+BB	694.90±51.50	-0.58±0.04	-2.45±0.12	38.53±4.73			1.77e-6±2.30e-8	1040/499
	Band+CPL	396.50±88.50	-0.40±0.07	-2.14±0.12		731.40±70.90	4.87±5.89	1.78e-6±2.40e-8	1046/498
130504978	Band	549.70±10.00	-1.20±0.01	-2.19±0.07				1.15e-6±1.00e-8	1781/482
	Band+BB	460.90±27.30	-1.05±0.03	-2.16±0.06	7.48±0.39			1.15e-6±1.00e-8	1744/480
	Band+PL	546.30±55.00	-1.19±0.08	-2.20±0.27			-1.78±5.43	1.15e-6±1.10e-8	1782/480
130518580	Band	390.30±12.00	-0.88±0.01	-2.34±0.07				1.32e-6±1.00e-8	790/484
	Band+BB	547.90±35.70	-1.00±0.03	-2.69±0.19	34.73±2.55			1.36e-6±1.30e-8	763/482
	Band+CPL	1433±604	-0.79±1.38	< 5		257.70±47.30	-0.82±0.19	1.34e-6±1.40e-8	756/481
130606497	Band	424.30±11.10	-1.18±0.01	-2.04±0.02				2.54e-6±1.00e-8	1990/481
	Band+BB	413.00±12.50	-1.08±0.02	-2.05±0.02	9.18±0.32			2.55e-6±1.00e-8	1839/479
	CPL+PL	473.10±15.10	-1.18±0.03				-1.44±0.08	2.60e-6±1.10e-8	2150/480
	Band+PL	431.00±21.30	-1.18±0.04	-2.05±0.06			-1.59±48.70	2.55e-6±2.40e-8	1991/479
131231198	Band	192.60±3.67	-1.25±0.01	-2.39±0.04				2.24e-6±9.30e-9	1630/484
	Band+BB	201.30±4.54	-1.17±0.02	-2.44±0.04	7.36±0.30			2.24e-6±9.40e-9	1514/482
140206275	Band	327.8±14.70	-1.23±0.01	-1.99±0.03				7.85e-7±9.40e-9	4044/484
	Band+BB	622.2±106.00	-1.41±0.02	-1.93±0.04	37.04±1.37			7.77e-7±6.80e-9	3967/482
	Band+PL	240.10±14.70	-1.01±0.07	-1.94±0.02			-3.17±0.49	7.78e-7±4.70e-9	3941/482
	CPL+BB+PL	348.00±35.20	-0.89±0.15		31.44±2.64		-1.64±0.02	7.73e-7±7.60e-9	3947/481
140329295	Band	218.50±6.12	-0.80±0.02	-2.20±0.03				1.93e-6±1.40e-8	971/360
	Band+BB	246.80±8.81	-0.68±0.04	-2.30±0.05	11.00±0.59			1.94e-6±1.50e-8	894/358
	CPL+BB+PL	351.90±14.20	-0.92±0.08		17.64±0.83		-1.45±0.75	1.99e-6±1.90e-8	956/357
140523129	Band	265.80±7.93	-1.08±0.01	-2.78±0.18				1.65e-6±1.40e-8	851/484
	Band+BB	269.00±9.25	-0.99±0.03	-2.82±0.19	8.64±0.68			1.65e-6±1.40e-8	824/482
	CPL+BB+PL	268.50±10.20	-0.93±0.12		9.05±0.84		-1.63±0.20	1.64e-6±1.70e-8	827/481
150201574	Band	120.80±2.04	-0.95±0.02	-2.54±0.04				1.92e-6±1.30e-8	917/484
	Band+BB	131.70±3.30	-0.90±0.03	-2.62±0.05	8.32±0.61			1.92e-6±1.30e-8	869/482
	Band+PL	121.90±2.11	-0.96±0.01	-2.60±0.55			-0.83±1.77	1.91e-6±1.70e-8	912/482
	CPL+BB+PL	137.10±2.89	-0.79±0.14		9.41±0.47		-1.66±0.10	1.85e-6±1.20e-8	894/481
150314205	Band	366.20±7.29	-0.73±0.01	-2.75±0.11				4.90e-6±3.50e-8	725/359
	Band+BB	447.40±15.80	-0.81±0.02	-3.43±0.44	29.38±2.06			5.01e-6±4.40e-8	681/357
	Band+PL	365.30±7.54	-0.73±0.01	-2.76±0.12			-0.15±13.90	4.89e-6±3.70e-8	725/357
150403913	Band	280.20±9.33	-0.49±0.03	-1.99±0.03				1.51e-6±1.30e-8	708/362

GRB	model	Band/CPL			BB	CPL/PL		$F_p / \text{keV s}^{-1} \text{cm}^{-2}$	C-stat/DOF
		$E_{\text{peak}}/\text{keV}$	α	β	kT/keV	$E_{\text{peak}}/\text{keV}$	p		
150627183	Band+BB	553.00 ± 33.80	-0.70 ± 0.03	-2.39 ± 0.10	24.86 ± 1.12			$1.60\text{e-}6 \pm 1.90\text{e-}8$	625/360
	Band+CPL	671.30 ± 61.10	-0.27 ± 1.57	-2.50 ± 0.14		127.10 ± 31.50	-0.14 ± 0.45	$1.62\text{e-}6 \pm 1.90\text{e-}8$	597/359
	Band	238.60 ± 4.71	-1.01 ± 0.01	-2.60 ± 0.03				$2.17\text{e-}6 \pm 1.00\text{e-}8$	1377/362
	Band+BB	241.60 ± 5.85	-0.92 ± 0.02	-2.23 ± 0.03	8.34 ± 0.43			$2.18\text{e-}6 \pm 1.10\text{e-}8$	1307/360
	Band+PL	224.40 ± 7.28	-1.02 ± 0.04	-2.22 ± 0.06			-1.68 ± 137	$2.17\text{e-}6 \pm 1.40\text{e-}8$	1427/360
150902733	CPL+BB+PL	355.50 ± 13.90	-1.14 ± 0.04		21.45 ± 1.00		-1.45 ± 0.35	$2.23\text{e-}6 \pm 1.40\text{e-}8$	1427/359
	Band	383.30 ± 7.98	-0.66 ± 0.15	-2.32 ± 0.04				$2.86\text{e-}6 \pm 1.80\text{e-}8$	939/483
	Band+BB	478.60 ± 19.70	-0.74 ± 0.02	-2.53 ± 0.08	30.36 ± 2.32			$2.92\text{e-}6 \pm 2.20\text{e-}8$	909/482
	Band+PL	396.50 ± 13.00	-0.68 ± 0.04	-2.36 ± 0.10			-1.2	$2.87\text{e-}6 \pm 1.50\text{e-}8$	941/482
151227218	Band+CPL	668.8 ± 520.00	-0.48 ± 3.49	-2.63 ± 0.17		196.20 ± 75.90	-0.56 ± 0.76	$2.93\text{e-}6 \pm 2.30\text{e-}8$	900/481
	Band	256.50 ± 17.10	-1.21 ± 0.02	-2.08 ± 0.06				$8.46\text{e-}7 \pm 8.70\text{e-}9$	1025/503
	Band+BB	243.50 ± 18.30	-1.01 ± 0.06	-2.09 ± 0.06	7.37 ± 0.44			$8.47\text{e-}7 \pm 8.90\text{e-}8$	982/502
151231443	CPL+BB+PL	292.80 ± 26.80	-1.07 ± 0.16		8.42 ± 0.58		-1.49 ± 0.28	$8.41\text{e-}7 \pm 1.30\text{e-}8$	994/501
	Band	185.40 ± 8.22		-2.14 ± 0.07				$9.96\text{e-}7 \pm 1.10\text{e-}8$	591/360
	Band+BB	178.20 ± 10.20	-0.35 ± 0.28	-2.41 ± 0.06				$9.91\text{e-}7 \pm 1.10\text{e-}8$	579/358
	Band+PL	186.70 ± 10.90	-0.90 ± 0.09	-2.48 ± 0.24			-1.38 ± 4.59	$9.95\text{e-}7 \pm 1.10\text{e-}8$	591/358
160422499	CPL+BB+PL	245.30 ± 18.50	-1.05 ± 0.22		25.59 ± 3.33		-1.61 ± 0.15	$9.58\text{e-}7 \pm 1.10\text{e-}8$	604/357
	Band	265.70 ± 6.22	-1.17 ± 0.01	-2.56 ± 0.09				$2.34\text{e-}6 \pm 1.50\text{e-}8$	1057/484
	Band+BB	275.40 ± 8.03	-1.15 ± 0.01	-2.63 ± 0.11	9.79 ± 1.35			$2.35\text{e-}6 \pm 1.50\text{e-}8$	1043/482
	Band+PL	266.70 ± 12.00	-1.17 ± 0.06	-2.57 ± 0.16			-1.48 ± 0.64	$2.34\text{e-}6 \pm 1.60\text{e-}8$	1057/482
	CPL+BB+PL	290.20 ± 11.90	-1.17 ± 0.05		11.31 ± 1.39		-1.48 ± 0.64	$2.36\text{e-}6 \pm 1.80\text{e-}8$	1048/481

3. THE ANALYSIS METHOD AND FITTING MODEL

The purpose of this paper is to investigate the simultaneous effect on the thermal component for the non-thermal component and the spectral evolution in whole prompt emission. Therefore, we should make sure the thermal component in the prompt emission spectra at first. We performed the time-integrated analysis in the main part of the prompt emission by the empirical Band function, and simultaneously fitted the same data with a combination of Band and each of functions as follows: *Blackbody (BB)*, power law (*PL*) and power law with exponential cutoff (*CPL*). When we add new component to Band, the C-stat value will decrease obviously, especially in Band+BB. Moreover, the values of C-stat are obtained in the two models. To distinguish which model is suitable for the spectra, we compared the decreasing C-stat per *DOF* (Δ C-stat) in the two model, and the Band+BB model get a better Δ C-stat. For the fitting time-integral spectrum, the variation range of the C-stat value is around 100. If the statistic value of the Band+BB fitting result decreases to 100 compared with the fitting of the Band model alone, it proves that there is thermal during the eruption. Some burst energy spectrum fitting results give a non-thermal component and so some bursts are excluded.

We showed the time-integrated fitting results in Table 2. In Table 2, the overall C-stat value of the time-integrated spectrum fitting results is generally several tens decreasing after adding the thermal component BB. On the other hand, when Band+CPL and Band+BB are fitted, the reduced values are not much different than those of the Band function fitting alone, and sometimes Band+CPL reduces the C-stat value more, so the unit degree of freedom C-stat/DOF is more appropriate. For example, in GRB150403913, compared with the fitting results of Band function alone, the overall C-stat value is reduced by 83 when Band+BB is fitted, and C-stat/DOF is 41.5; the reduced value when fitted by Band+CPL is 111, while the C-stat/DOF is 37. We remove some burst due to the lack of thermal component in the prompt emission time-integrated spectra. There are four empirical functions in our spectral fitting, which are listed as follows:

The Band (Band) model is defined as (i.e. Band function)

$$f_{\text{band}}(E) = A \begin{cases} \left(\frac{E}{100\text{keV}}\right)^\alpha \exp\left(-\frac{(\alpha+2)E}{E_p}\right), & E < \frac{(\alpha-\beta)E_p}{(\alpha+2)} \\ \left(\frac{E}{100\text{keV}}\right)^\beta \exp(\beta-\alpha) \frac{(\alpha-\beta)E_p}{100\text{keV}(\alpha+2)}^{\alpha-\beta}, & E \geq \frac{(\alpha-\beta)E_p}{(\alpha+2)} \end{cases}$$

where A is the normalization factor at 100keV in units of $\text{phs cm}^{-2}\text{keV}^{-1}$; α and β are the low-energy and high-energy power-law (PL) index, respectively; E_p is the peak energy in units of keV.

The blackbody (BB) model is defined as (i.e. Planck function)

$$f_{\text{BB}}(E) = A \frac{\left(\frac{E}{\text{keV}}\right)^2}{\exp\left(\frac{E}{kT}\right) - 1}$$

where A is the normalization factor at 1 keV; kT is the blackbody temperature in units of keV

The power-law with an exponential cutoff (CPL) is defined as (i.e. Compton function)

$$f_{\alpha}(E) = A \left(\frac{E}{100 \text{ keV}} \right)^{\alpha} \exp\left(-\frac{(\alpha+2)E}{E_p}\right)$$

where A is the normalization factor at 100 keV in units of phs cm⁻² keV⁻¹; α is the lower-energy power-law index; E_p is the peak energy in units of keV.

The power-law model (PL) is defined as

$$f_p(E) = A \left(\frac{E}{100 \text{ keV}} \right)^p$$

where A is the normalization factor at 100 keV; p is the power law index.

4. MULTI-COMPONENT MODEL FITTING RESULTS

We first fit the time-integrated spectra of our sample with two-component model which is a combination of Band and each of *CPL*, *BB* and *PL*, and a new multi-component model *CPL+BB+PL*, which has been presented in Guiriec et al. (2015a). We must point out that the thermal component can be modeled in time-resolved spectra in most of bursts which we selected, and Burgess et al. (2014a) showed that the important information of the spectra will be covered in the time-integrated spectra.

In Table 2 the parameters of Band function surround the characteristic value, the low-energy power-law index $\alpha \sim -1$, the high-energy power-law index $\beta \sim -2.2$, the results are very consistent with Preece et al. (1998). When we add BB into Band, α becomes softer, β is slightly smaller and E_p increases significantly in individual burst. Additionally, the peak flux of νF_{ν} spectra F_p is same in all fitting model. Comparing the fitting results with Band+BB and *CPL+BB+PL*, the parameters of the two models are similar and the index of PL component of *CPL+BB+PL* model is closed to -1.5 compared with Band+PL model.

4.1 Band and Band+BB model

In time-resolved analysis, we have shown the distributions of the three parameters in Figure 1 and the red curve in which is the Gaussian Fitting. And we also present the Gaussian Fitting results in Table 3. For the individual burst, α decrease when add BB into Band, but in a few time intervals it will increase. It will decrease after the first rising and there seems a linear correlation in the decays of α (see Figure 1). For the overall sample, the α of the Band+BB spectra is softer than that of Band only (see, Table 3, Figures 1 and 2).

Table 3 Gauss fitting results of frequency distribution statistics of each parameter in different model

Model	parameter	x_c	r^2
Band	α	-0.75 ± 0.01	0.9541
	β	-2.42 ± 0.01	0.9499
	E_p / keV	208.38 ± 8.54	0.9603
Band+BB	α	-0.87 ± 0.01	0.9905
	β	-2.57 ± 0.02	0.9216
	E_p / keV	278.97 ± 7.55	0.9231

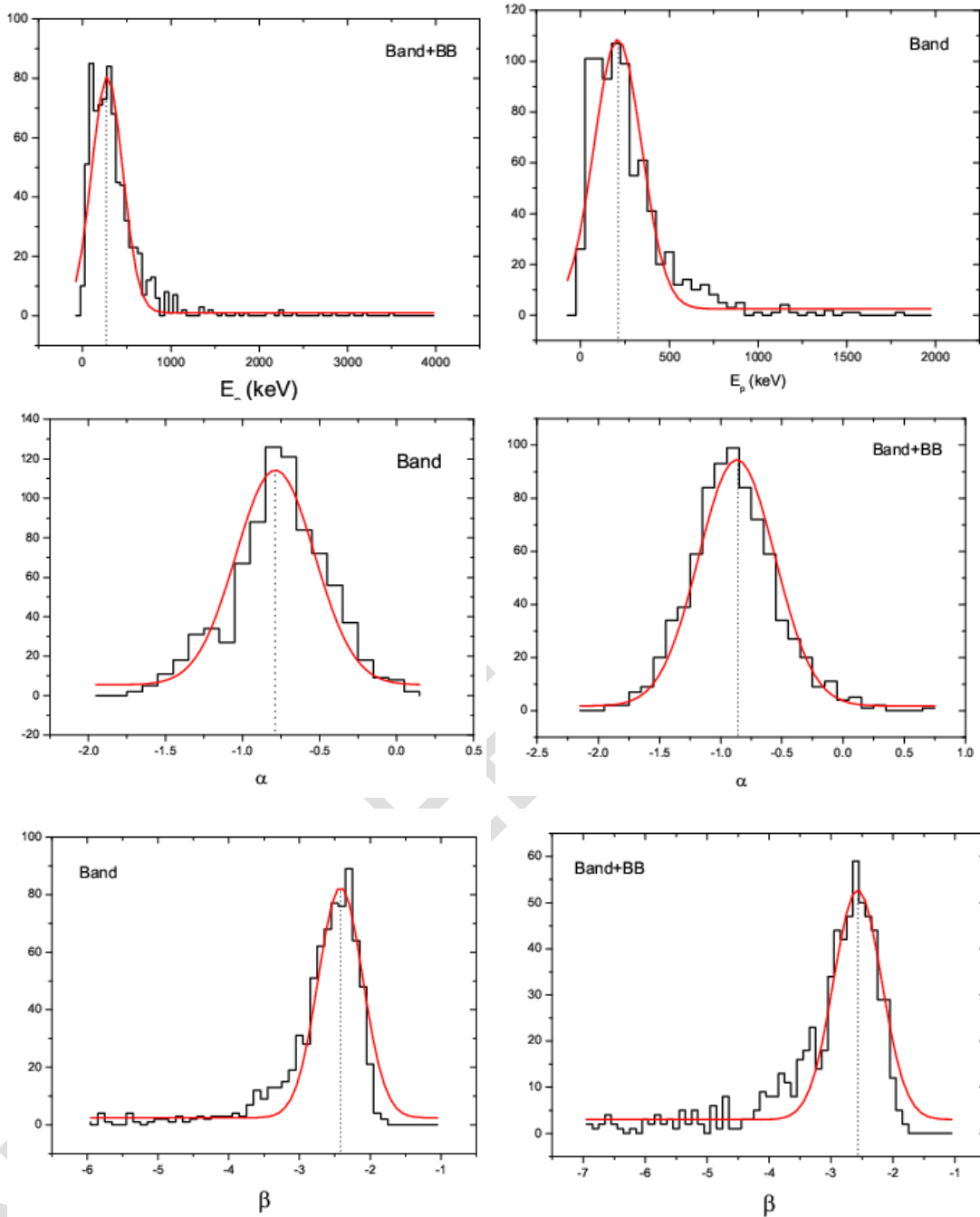


Fig. 1 The distributions of spectral parameters in different models, and the red solid line are Gaussian fitting curve. Left panels: Band models. Right panels: Band+BB models.

The mean value of β is slightly smaller in Band+BB than that in Band, and it will suddenly shift to a small value (<5) in several time intervals. Besides, the evolution with time is similar in the two models (see Figure 3).

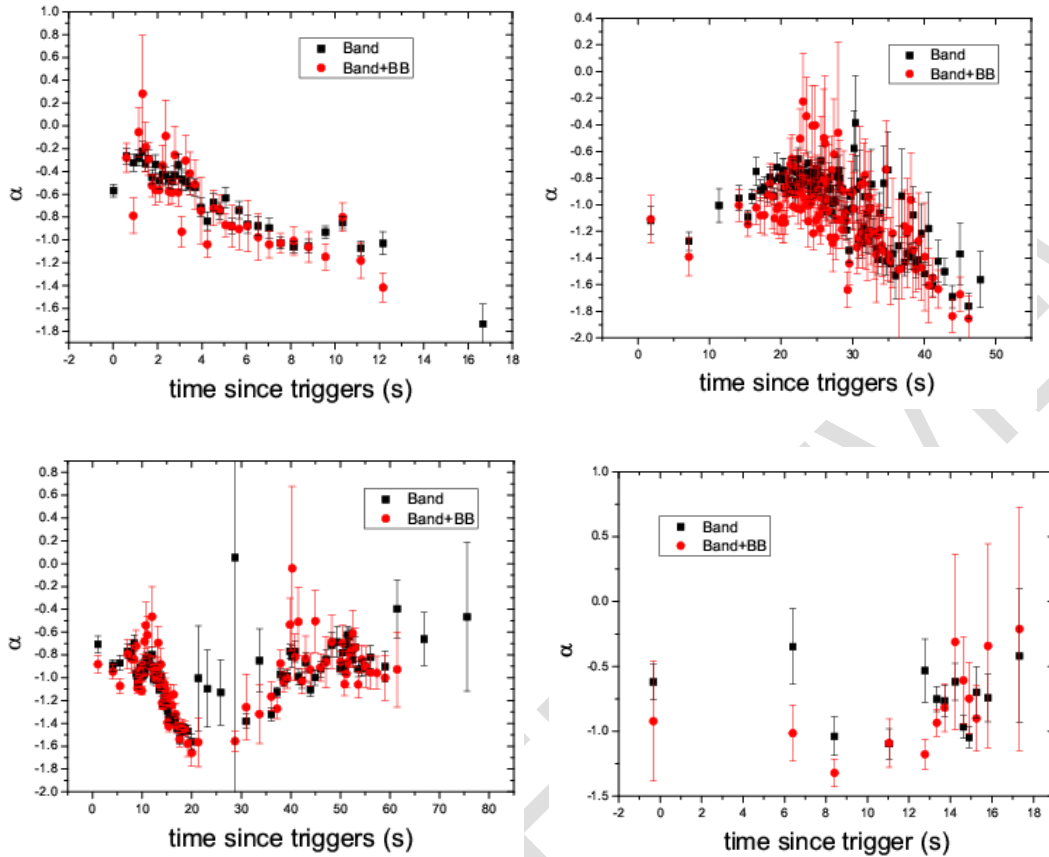


Fig. 2 The α evolution with time of the parameters in two different fitting models. Band only: the *black squares*; Band+BB: filled *red circle*. Top left : GRB150314205, Bottom left : GRB130606497, Top right : GRB131231198, Bottom right : GRB120707800.

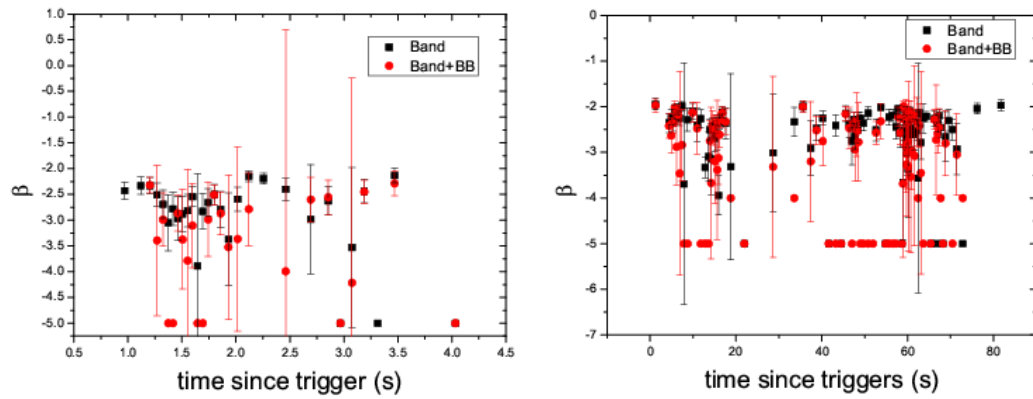


Fig. 3 The β evolution with time of the parameters in two different models. Band only: the *black squares*; Band+BB: filled *red circle*.

The peak energy E_p of vF_v spectra increases significantly after adding BB to Band function and the decay of E_p is faster in Band+BB (see Figure 4) due to the thermal component

(Huang et al. 2016). Besides, F_p is similar in the two model (see, Figure 5). These results are very consistent with previous research (e.g. Huang et al. 2016).

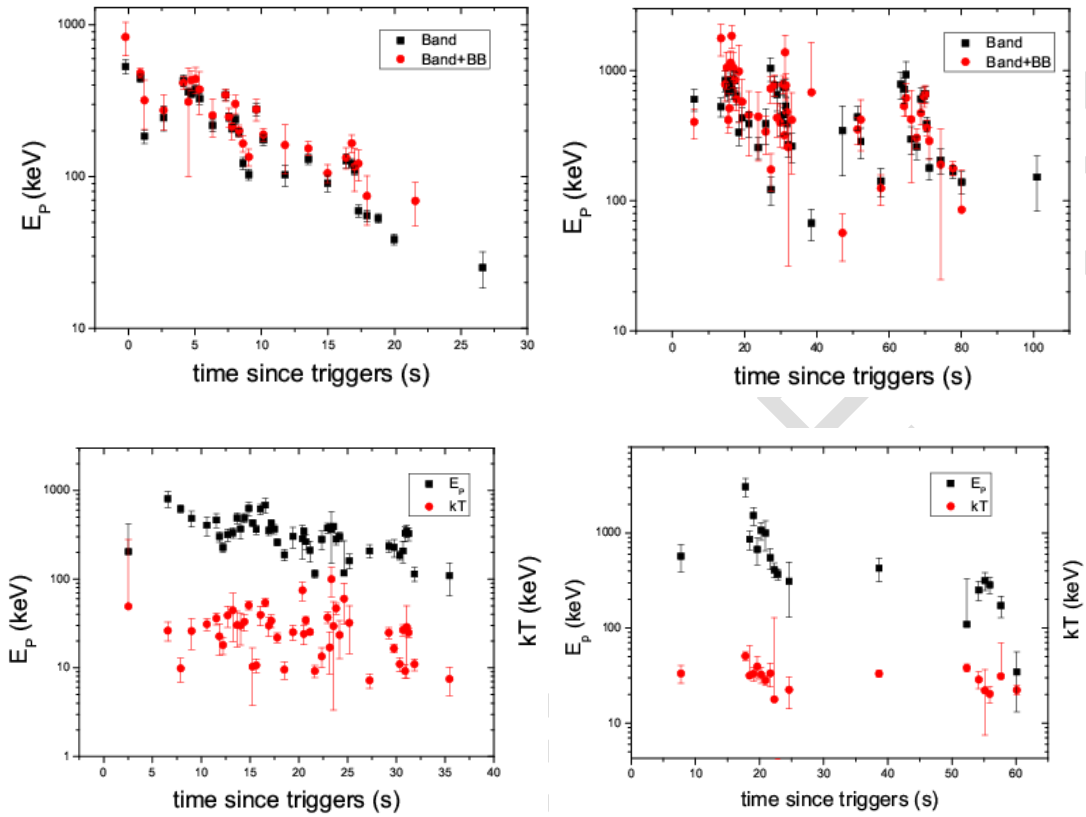


Fig. 4 The E_p evolution with time and the thermal temperature kT fitting with Band+BB; E_p : the *black squares*; kT : filled *red circle*. Top left: GRB140523129, Bottom left: GRB130502327, Top right: GRB130504978, Bottom right: GRB121225417.

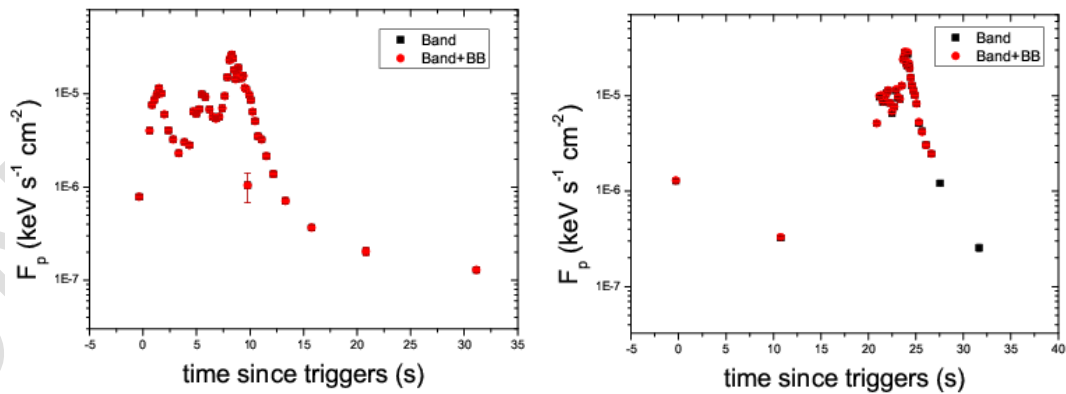


Fig. 5 The F_p evolution with time in two different fitting models. Band only: the *black squares*; Band+BB: the *red circle*. Left panel: GRB160422499, right panel: GRB140329295.

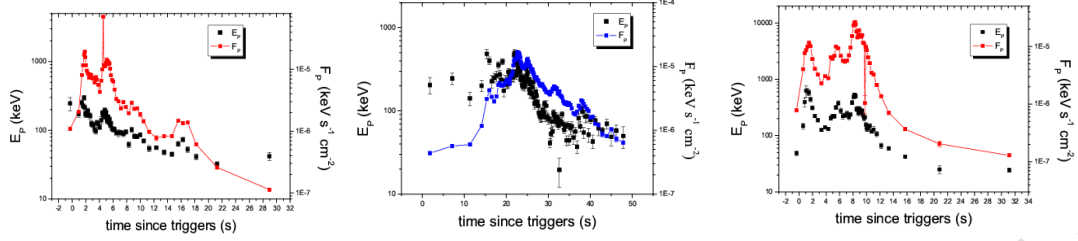


Fig. 6 The evolution with time of the peak energy E_p and the energy flux F_p fitting with Band+BB; E_p : the black squares; F_p : filled red squares. Left panel : GRB150201574 ; middle panel : GRB 131231198 ; down panel : GRB160422499

Previous study showed that there is a positive correlation between peak energy E_p and α and the decay of peak energy E_p follows a relation with time, $E_p \propto t^{-\delta}$, during the decay pulse (Crider et al. 1997; Daigne & Mochkovitch 2003; Peng et al. 2009). In this work the same evolution trends have been found between E_p and peak flux F_p . Compared the evolution process of the two parameters, there are two types of evolutionary form, “Hard-to-Soft” and “Tracking”. If the evolution of E_p follows the evolution of F_p , then the evolution of E_p takes on the form of “Tracking”, such as GRB160422499; if the evolution of E_p exhibits a maximum value at the beginning of the explosion and then decays over time, the evolution of E_p at this case is inconsistent with the evolution of F_p , showing the form of “from hard to soft”, such as GRB140523129; but in our fitting results, we noticed that in GRB150201574, the evolution of E_p follows the form of “from hard to soft” in the rise phase, but the form of “Tracking” appears in the attenuation process, as shown in Figure 6.

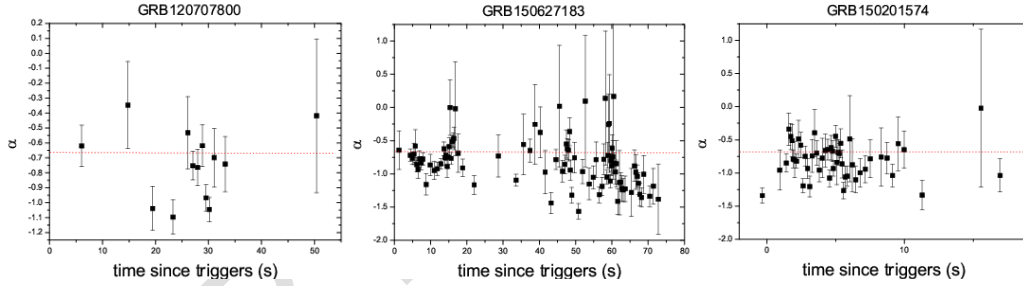


Fig. 7 Fitting result of low-energy power law index α more than $-2/3$ scale diagram; the red line is $\alpha=-2/3$.

4.2 CPL+BB+PL model

The new model CPL+BB+PL has been showed in Guiriec et al. (2015a), and the parameters of which can be compared with Band+BB model. Only for GRB120129580, 121225417, 130504978, 14026275, 140329295, 150201574, 150627183, 151227218, 151231443, 160422499, the CPL+BB+PL model can get the fitting results, but some components will have large errors, and we notice that the model could not fit in most of the time intervals for the time-resolved spectra in these GRBs; the model does not appear in the GRB120707800 time-integrated spectra, but a better fitting result was obtained in the time-resolved spectra. If the model is artificially constructed, why does it only appear in the time-resolved spectrum? Burgess et al. (2014a) pointed out that the time-integrated spectrum tends to cover up some important information in the energy spectrum. Therefore, it is recommended to use the time-resolved spectrum as much as possible in the energy spectrum analysis.

In the time-resolved spectrum analysis, only the four bursts of GRB120707800, 121225417, 140329295, 151231443 can be well fitted, and we noticed that the CPL+BB+PL model parameters E_p , kT and p and Band+BB model parameters, E_p , and kT are similar, so we can try to limit the value of each parameter in the CPL+BB+PL model so that it can be compared with the Band+BB model. Comparing the same parameters under the two models, the parameters E_p , and kT in the CPL+BB+PL model are slightly larger than those in the Band+BB model.

It can be seen from Table 4 that the low-energy spectrum index is not unique in the time-resolved spectrum fitting of each burst. In the time-integrated spectrum of GRB120707800, 121225417, and 140329295, it fluctuates at -1, -1.1, and -0.8 respectively, which are noted as CPL_{-1} , $CPL_{-1.1}$, $CPL_{-0.8}$; the value of GRB151231443 fluctuates greatly. In the low energy range, the Band spectrum has the same spectrum shape as the CPL spectrum. Under the limit of synchrotron radiation, the electron index of fast cooling and slow cooling processes correspond to -0.7 and -1.5. As discussed in Section 4.1, our limit value should be less than -0.7, and we assume $\alpha = -0.7$ of GRB151231443, recorded as $CPL_{-0.7}$. The thermal energy kT fluctuates in dozens of keV; the value of the power-law spectrum index p is between -1 and -2, so we choose the power-law spectrum index $p=-1.5$, which is recorded as $PL_{-1.5}$ (see Table 4). In the time-integrated spectrum fitting results, the CPL+BB+PL low-energy power-law index is less than -1, and close to -1 in a few GRBs. The thermal energy kT and the power-law index p are similar to the results of the time-resolved spectrum.

After limiting α and p , the model is recorded as $CPL_{fix} + BB + PL_{-1.5}$, which reduces 2 degrees of freedom, and the value of C-stat/DOF is very close to Band+BB. The fitting results are given in Table 4. But we must point out that the CPL+BB+PL model and $CPL_{fix} + BB + PL_{-1.5}$ model can get the fitting results in some time intervals, but only the latter can be used in some intervals. It is worth noting that the PL component also appears in the energy spectrum at the beginning of the fireball explosion. The PL component can also explain why the initial low-energy power law index is often less than -1 when the CPL+BB+PL model is fitted. Only in the energy spectrum fitting can we first observe the PL component.

We try to compare Band+BB, CPL+BB+PL, and $CPL_{fix} + BB + PL_{-1.5}$ and the changes of each parameter under these models. When the three models can be used together to fit the time-resolved spectrum, the changes of various parameters, E_p , and kT seem to be insignificant, but there will be mutations in a small number of time-resolved spectra. However, we must point out that when using CPL+BB+PL to fit the time-resolved spectrum, most of the PL components in the energy spectrum have large errors. Therefore, not all time-resolved spectra can be fitted with CPL+BB+PL.

Table 4 Time-resolved spectrum fitting results for 20 bursts

GRB	T-start (s)	T-end (s)	模型	Band/CPL			BB	PL	F _p /keV s ⁻¹ cm ⁻²	Cstat/DOF
				E _p /keV	α	β	kT/keV	ρ		
120707800	-0.64	12.795	Band	204.0±157.0	-0.62±0.14	-2.03±0.05			1.33e-6±2.80e-8	581/360
			Band+BB	408.2±111.0	-0.92±0.46	-2.02±0.08	19.76±5.85		1.33e-6±2.90e-8	581/358
			CPL+BB+PL	308.7±36.0	-1.23±0.20		23.56±2.19	-1.44±0.45	1.35e-6±3.50e-8	582/457
	12.795	16.811	CPL _{-1.0} +BB+PL _{-1.5}	80.69±11.8	-1.0		20.86±1.53	-1.5	1.32e-6±3.30e-8	584/359
			Band	238.0±59.0	-0.35±0.29	-2.06±0.05			1.88e-6±5.40e-8	478/360
			Band+BB	239.3±36.2	-1.02±0.22	-2.38±0.25	13.42±1.86		1.88e-6±5.70e-8	473/358
	16.811	22.086	CPL+BB+PL	244.0±33.3	-0.23±1.42		13.98±1.69	-1.74±0.12	1.84e-6±6.10e-8	473/357
			CPL _{-1.0} +BB+PL _{-1.5}	113.0±18.3	-1.0		13.71±1.04	-1.5	1.85e-6±6.10e-8	474/359
			Band	236.0±33.8	-1.04±0.15	-2.23±0.10			1.54e-6±4.70e-8	531/360
	22.086	25.540	Band+BB	204.5±31.2	-1.32±0.11	<5	13.95±2.71		1.54e-6±5.50e-8	527/358
			CPL+BB+PL	185.9±22.4	-1.26±0.13		12.95±2.94	0.85±1.59	1.48e-6±6.60e-8	521/357
			CPL _{-1.0} +BB+PL _{-1.5}	159.8±25.9	-1.0		10.28±1.13	-1.5	1.49e-6±4.70e-8	528/359
	25.540	26.672	Band	136.6±94.2	-1.10±0.12	-2.33±0.17			2.37e-6±7.50e-8	424/360
			Band+BB	181.8±17.1	-1.09±0.19	-2.25±0.38	57.5±37.0		2.35e-6±8.40e-8	425/358
			CPL+BB+PL	194.9±23.5	-0.29±1.01		9.27±1.63	-1.62±0.23	2.26e-6±7.70e-8	418/357
	26.672	27.441	CPL _{-1.0} +BB+PL _{-1.5}	100.8±16.5	-1.0		9.79±1.86	-1.5	2.29e-6±7.50e-8	420/359
			Band	389.3±60.7	-0.53±0.24	-2.03±0.06			2.82e-6±8.00e-8	385/360
			Band+BB	347.2±58.7	-1.18±0.11	<-5	15.99±1.82		2.94e-6±9.40e-8	379/358
	27.441	28.453	CPL+BB+PL	318.6±42.3	-1.15±0.12		15.75±1.90	0.11±1.85	2.78e-6±1.10e-7	372/357
			CPL _{-1.0} +BB+PL _{-1.5}	230.7±22.9	-1.0		14.70±1.14	-1.5	2.87e-6±9.40e-8	377/359
			Band	385.1±40.3	-0.75±0.10	-2.43±0.15			6.78e-6±1.80e-7	381/360
	28.453	29.235	Band+BB	360.1±45.0	-0.93±0.10	<-5	21.69±3.43		6.99e-6±2.00e-7	372/358
			CPL+BB+PL	399.0±38.7	-0.91±0.11		21.50±3.60	1.07±2.54	6.85e-6±2.40e-7	369/357
			CPL _{-1.0} +BB+PL _{-1.5}	171.0±20.6	-1.0		24.06±2.77	-1.5	6.99e-6±2.50e-7	368/359
	29.235	29.812	Band	278.5±31.4	-0.76±0.12	-2.34±0.13			5.03e-6±1.40e-7	398/360
			Band+BB	285.7±26.5	-0.82±0.19	-3.29±0.92	14.41±2.18		5.04e-6±1.50e-7	389/358
			CPL+BB+PL	297.6±31.7	-0.87±0.15		15.29±2.23	-0.66±1.19	5.02e-6±1.60e-7	386/357
	29.812	30.511	CPL _{-1.0} +BB+PL _{-1.5}	157.1±18.5	-1.0		18.59±2.08	-1.5	5.09e-6±1.50e-7	389/359
			Band	160.5±25.1	-0.62±0.14	-2.33±0.17			5.68e-6±1.60e-7	367/360
			Band+BB	190.6±20.3	-0.31±0.68	-2.36±0.13	8.35±2.43		5.65e-6±1.60e-7	365/358
	30.511	31.616	CPL+BB+PL	230.3±25.8	-0.55±0.48		15.98±7.60	-1.503±0.23	5.42e-6±1.70e-7	358/357
			CPL _{-1.0} +BB+PL _{-1.5}	224.9±23.5	-1.0		29.04±4.46	-1.5	5.55e-6±1.70e-7	362/359
			Band	249.0±31.1	-0.97±0.09	-2.56±0.21			7.70e-6±2.10e-7	419/360
	31.616	34.655	Band+BB	249.0±31.1	-0.97±0.09	-2.63±0.24	11.68±1.58		7.67e-6±2.10e-7	411/358
			CPL+BB+PL	280.0±28.3	-0.61±0.33		13.21±1.80	-1.46±0.73	7.65e-6±2.30e-7	410/357
			CPL _{-1.0} +BB+PL _{-1.5}	296.7±30.0	-0.78±0.35		16.03±2.36	-1.5	7.73e-6±2.30e-7	412/359
	34.655	66.112	Band	249.5±28.4	-1.0				6.70e-6±1.90e-7	452/360
			Band+BB	270.9±36.8	-1.04±0.08	-2.56±0.24	11.70±1.74		6.68e-6±1.90e-7	445/358
			CPL+BB+PL	289.9±30.9	-0.75±0.28	-2.62±0.27	12.99±2.16	0.84±1.22	6.50e-6±2.50e-7	434/357
	66.112	-1.984	CPL _{-1.0} +BB+PL _{-1.5}	309.2±33.3	-0.90±0.17		15.04±2.23	-1.5	6.73e-6±2.00e-7	444/359
			Band	115.8±18.6	-1.0				4.25e-6±1.20e-7	399/360
			Band+BB	217.5±40.5	-0.70±0.20	-2.12±0.09	12.87±2.69		4.26e-6±1.30e-7	394/358
	-1.984	17.482	CPL+BB+PL	265.0±40.5	-0.90±0.25	-2.37±0.20	14.53±2.23	-1.12±0.57	4.22e-6±1.40e-7	390/357
			CPL _{-1.0} +BB+PL _{-1.5}	106.2±15.0	-1.0		14.56±1.55	-1.5	4.22e-6±1.40e-7	390/359
			Band	126.6±27.5	-0.74±0.18				2.09e-6±6.50e-8	482/360
	17.482	18.126	Band+BB	170.8±21.8	-0.34±0.78		8.51±1.91		2.07e-6±6.60e-8	479/358
			CPL+BB+PL	179.2±23.6	-0.76±0.50		11.58±2.00	-1.52±0.30	2.00e-6±7.00e-8	477/359
			CPL _{-1.0} +BB+PL _{-1.5}	43.1±7.5	-1.00		13.76±1.77	-1.5	2.02e-6±6.40e-8	478/359
18.126	18.776	Band	33.9±9.6	-0.42±0.51	-2.07±0.05			4.74e-7±1.60e-8	846/360	
		Band+BB	105.5±17.4	-0.21±0.94	-2.04±0.07	23.76±6.72		4.72e-7±1.70e-8	841/358	
		CPL+BB+PL	381.2±48.1	-1.00		6.93±0.81	-1.5	4.52e-7±1.50e-8	827/359	
18.776	19.312	CPL _{-1.0} +BB+PL _{-1.5}	572.1±185.0	-0.96±0.05	-2.19±0.21			6.34e-7±1.90e-8	500/504	
		Band	591.9±197.0	-1.09±0.09	-2.36±0.40	33.131±7.06		6.50e-7±2.70e-8	498/502	
		Band+BB	646.3±86.6	-1.08±0.32		33.12±8.49	-1.45±1.04	6.57e-7±2.20e-8	499/501	
19.312	19.970	CPL _{-1.1} +BB+PL _{-1.5}	502.3±75.3	-1.1		33.89±4.98	-1.5	6.59e-7±2.20e-8	499/503	
		Band	3078.0±681.0	-0.68±0.07	-1.81±0.07			5.43e-6±1.70e-7	580/504	
		Band+BB	791.6±116.0	-1.06±0.04	-2.67±0.57	50.89±4.99		5.38e-6±1.70e-7	572/502	
19.970	20.516	Band	860.7±193.0	-0.94±0.04	-2.56±0.40			5.17e-6±1.70e-7	546/504	
		Band+BB	1335.0±196.0	-0.96±0.07	-2.64±0.49	31.61±33.9		5.16e-6±1.70e-7	545/502	
		CPL+BB+PL	682.8±107.0	-1.1		61.6±12.2	-1.5	5.03e-6±1.50e-7	550/503	
20.516	21.296	CPL _{-1.1} +BB+PL _{-1.5}	1532.0±325.0	-0.99±0.04	-2.31±0.26			5.61e-6±2.10e-7	561/504	
		Band	1454.0±220.0	-1.17±0.04	<-5	32.98±5.35		5.56e-6±1.90e-7	552/502	
		Band+BB	473.7±62.8	-1.1		32.39±4.74	-1.5	5.57e-6±1.70e-7	552/503	
21.296	22.062	CPL _{-1.1} +BB+PL _{-1.5}	670.8±210.0	-0.85±0.05	-2.22±0.19			4.74e-6±1.70e-7	528/504	
		Band	1093.0±174.0	-0.97±0.10	-2.32±0.28	39.43±10.50		4.79e-6±1.80e-7	526/502	
		Band+BB	548.9±75.7	-1.1		45.34±5.17	-1.5	4.74e-6±1.50e-7	532/503	
22.062	22.551	CPL _{-1.1} +BB+PL _{-1.5}	1071.0±227.0	-0.26±0.05	-2.36±0.28			5.48e-6±2.10e-7	584/504	
		Band	1163.0±168.0	-1.07±0.05	<-5	32.43±6.10		5.61e-6±1.80e-7	579/502	
		Band+BB	257.3±38.1	-1.1		33.79±5.28	-1.5	5.71e-6±1.70e-7	581/503	
22.551	23.117	Band	998.8±346.0	-0.94±0.08	-1.91±0.09			3.48e-6±1.10e-7	572/504	
		Band+BB	1103.0±399.0	-1.11±0.07	-2.55±0.61	28.22±3.31		3.76e-6±1.30e-7	561/502	
		CPL+BB+PL	1093.0±211.0	-1.1±0.35		28.63±3.32	-1.51±1.08	3.76e-6±1.40e-7	561/501	
23.117	26.126	CPL _{-1.1} +BB+PL _{-1.5}	428.9±59.5	-1.1		28.56±2.63	-1.5	3.77e-6±1.30e-7	561/503	
		Band	549.8±136.0	-0.88±0.05	-2.90±0.91			3.76e-6±1.60e-7	583/504	
		Band+BB	768.1±111.0	-0.97±0.10	-3.08±1.54	33.38±9.40		3.81e-6±1.60e-7	580/502	
26.126	51.129	CPL+BB+PL	406.7±47.7	-1.1		37.86±5.33	-1.5	3.91e-6±3.30e-7	585/503	
		Band	409.5±72.0	-0.78±0.06	-2.40±0.27			5.44e-6±1.90e-7	564/504	
		Band+BB	740.0±122.0	-0.78±0.10	-2.41±0.29	17.77±111.0		5.44e-6±2.10e-7	564/502	
51.129	53.507	CPL _{-1.1} +BB+PL _{-1.5}	388.9±42.1	-1.1		57.16±5.90	-1.5	5.40e-6±1.90e-7	570/503	
		Band	369.2±48.0	-0.75±0.06	-2.49±0.31			5.02e-6±1.80e-7	629/504	
		Band+BB	633.9±108.0	-0.68±0.12	-2.48±0.30	3.86±2.63		5.00e-6±1.80e-7	628/502	
53.507	54.872	CPL+BB+PL	215.5±41.2	-1.1		61.4±5.76	-1.5	4.95e-6±1.80e-7	632/503	
		Band	311.3±182.0	-1.06±0.08	-2.00±0.14			1.15e-6±4.40e-8	554/504	
		Band+BB	492.0±287.0	-1.19±0.18	-2.05±0.22	22.43±8.32		1.16e-6±4.40e-8	553/502	
54.872	55.428	CPL+BB+PL	296.8±40.3	-1.29±0.45		23.90±4.98	-1.49±1.76	1.20e-6±6.20e-8	554/501	
		CPL _{-1.1} +BB+PL _{-1.5}	222.6±20.2	-1.1		19.66±5.03	-1.5	1.14e-6±5.20e-8	555/503	
		Band	427.2±118.0	-0.92±0.05	-2.42±0.29			4.85e-7±1.70e-8	707/504	
55.428	56.387	Band+BB	394.4±104.0	-1.27±0.09	<-5	33.10±2.76		4.98e-7±2.00e-8	704/502	
		CPL+BB+PL	285.8±29.7	-1.25±0.09		33.66±2.91	-0.06±3.74	4.92e-7±2.10e-8	703/501	
		CPL _{-1.1} +BB+PL _{-1.5}	210.2±36.1	-1.1		33.82±4.66	-1.5	4.79e-7±1.80e-8	705/503	
56.387	58.872	Band	109.6±222.0	-1.09±0.07	-2.23±0.27			1.16e-6±5.50e-8	579/504	
		Band+BB	95.8±514.0	-1.45±0.32	-1.75±0.11	38.05±3.63		1.11e-6±4.80e-8	563/502	
		CPL+BB+PL	45.54±21.4	-0.74±6.94		40.66±16.7	-1.70±0.18	1.09e-6±5.70e-8	563/501	
58.872	59.428	CPL _{-1.1} +BB+PL _{-1.5}	206.9±15.4	-1.1		41.81±4.46	-1.5	1.06e-6±4.70e-8	564/503	
		Band	252.1±55.8	-0.83±0.06	<-5			1.64e-6±7.20e-8	557/504	
		Band+BB	287.2±30.2	-1.01±0.16	<-5	28.70±5.77		1.69e-6±1.00e-7	555/502	
59.428	59.872	Band	316.7±66.7	-0.85±0.06	-2.74±0.56			4.09e-6±1.50e-7	529/504	
		Band+BB	314.							

GRB	T-start (s)	T-end (s)	模型	Band/CPL			BB	PL	F _p /keV s ⁻¹ cm ⁻²	Cstat/DOF
				E _p /keV	α	β	kT/keV	ρ		
140329295	56.387	58.909	Band	173.0±44.3	-0.96±0.07	-2.99±0.99			9.77e-7±6.50e-8	596/504
			Band+BB	85.3±8.1	-1.00±0.21	-2.88±1.03	31.08±28.50		9.79e-7±6.40e-8	596/502
	58.909	61.306	Band	34.6±21.4	-1.17±0.09	-3.02±0.75			6.68e-7±5.10e-8	572/504
			Band+BB	87.1±11.0	-1.32±0.46	-2.10±0.17	22.24±2.55		7.06e-7±4.60e-8	567/502
	61.306	63.249	Band	59.84±5.62	-1.38±0.09	-2.79±0.67			7.97e-7±6.10e-8	501/504
			CPL _{-1.1} +BB+PL _{-1.5}	79.8±9.9	-1.1		9.65±1.21	-1.5	7.82e-7±4.80e-8	500/503
	63.249	66.301	Band	76.9±8.7	-1.45±0.09	-2.79±0.68			6.04e-7±4.70e-8	514/504
			CPL _{-1.1} +BB+PL _{-1.5}	26.6±2.8	-1.1		18.25±2.71	-1.5	5.60e-7±3.80e-8	514/503
	66.301	85.312	CPL _{-1.1} +BB+PL _{-1.5}	507.5±38.3	-1.1		7.64±0.79	-1.5	1.57e-7±1.20e-8	534/503
			Band	143.1±16.6	-0.38±0.15	-2.17±0.12			1.28e-6±5.40e-8	382/360
			Band+BB	327.8±127.0	-0.95±0.20	-2.53±0.68	23.9±3.19		1.29e-6±6.20e-8	382/358
			CPL+BB+PL	373.4±123.0	-0.99±0.49		24.25±3.07	-1.45	1.31e-6±3.90e-8	382/357
			CPL _{-0.8} +BB+PL _{-1.5}	298.2±38.7	-0.8		22.45±2.29	-1.5	1.28e-6±6.10e-8	384/359
			Band	264.3±52.1	-0.80±0.12	-2.11±0.22			3.24e-7±1.60e-8	535/360
	0.842	20.686	Band	314.5±81.0	-0.45±0.40	-2.21±0.31	13.19±1.97		3.32e-7±1.70e-8	326/358
			Band+BB	414.5±102.0	-0.71±0.72		15.20±2.66	-1.44	3.40e-7±2.20e-8	529/357
			CPL+BB+PL	225.6±23.3	-0.81±0.08	-2.68±0.36			5.13e-6±2.00e-7	377/360
	20.686	21.054	Band	239.2±30.3	-0.66±0.19	-2.76±0.42	10.75±2.62		5.14e-6±2.00e-7	373/358
			Band+BB	243.5±22.6	-0.32±0.67		11.97±2.44	-1.67±0.19	5.01e-6±2.10e-7	374/357
			CPL+BB+PL	264.8±23.4	-0.8		13.01±2.44	-1.5	5.12e-6±2.10e-7	375/359
			CPL _{-0.8} +BB+PL _{-1.5}	217.9±22.7	-0.61±0.09	-2.31±0.15			9.370e-6±3.20e-7	358/360
	21.054	21.256	Band	343.8±58.9	-0.70±0.14	-2.67±0.40	18.15±2.62			346/358
			Band+BB	379.8±50.6	-0.74±0.36		19.16±2.32	-1.44±1.81	9.91e-6±3.60e-7	349/357
			CPL+BB+PL	402.3±39.2	-0.8		20.13±1.81	-1.5	1.00e-5±3.80e-7	349/359
			CPL _{-0.8} +BB+PL _{-1.5}	191.3±22.0	-0.62±0.10	-2.26±0.13			1.00e-5±3.70e-7	367/360
	21.256	21.435	Band	276.7±47.7	-0.67±0.16	-2.51±0.27	15.17±2.99		9.94e-6±3.30e-7	360/358
			Band+BB	380.5±53.0	-0.88±0.40		19.54±2.70	-1.66	1.10e-5±3.60e-7	365/357
			CPL+BB+PL	350.5±33.0	-0.8		17.91±1.82	-1.5	1.04e-5±4.00e-7	365/359
			CPL _{-0.8} +BB+PL _{-1.5}	163.8±17.6	-0.43±0.12	-2.23±0.11			1.03e-5±3.90e-7	380/360
	21.435	21.648	Band	310.2±61.3	-0.76±0.15	-2.73±0.46	19.89±3.19		8.53e-6±2.80e-7	373/358
			Band+BB	368.3±56.8	-0.88±0.34		21.42±2.66	-1.46	8.71e-6±3.20e-7	376/357
			CPL+BB+PL	351.6±33.4	-0.8		20.53±1.82	-1.5	8.88e-6±3.50e-7	376/359
			CPL _{-0.8} +BB+PL _{-1.5}	219.3±22.6	-0.71±0.08	-2.51±0.22			8.85e-6±3.40e-7	389/360
	21.648	21.819	Band	208.2±27.3	-0.21±0.43	-2.64±0.19	9.23±1.19		1.00e-5±3.50e-7	383/358
			Band+BB	309.2±45.0	-0.88±0.15		22.12±6.76	-1.30	1.00e-5±3.50e-7	389/357
			CPL+BB+PL	307.5±25.5	-0.8		15.39±2.67	-1.5	1.02e-5±4.00e-7	388/359
			CPL _{-0.8} +BB+PL _{-1.5}	271.6±31.9	-0.86±0.07	-2.44±0.22			1.03e-5±4.00e-7	411/360
	21.819	21.997	Band	253.1±35.1	-0.26±0.40	-2.42±0.19	9.52±0.86		1.06e-5±3.60e-7	397/358
			Band+BB	365.7±36.9	-0.77±0.36		11.45±2.01	-1.543	1.06e-5±3.60e-7	405/357
			CPL+BB+PL	292.5±23.6	-0.8		15.82	-1.5	1.11e-5±4.20e-7	421/359
			CPL _{-0.8} +BB+PL _{-1.5}	244.1±25.1	0.76±0.07	-2.89±0.43			1.07e-5±3.90e-7	353/360
	21.997	22.147	Band	314.3±57.6	-0.89±0.13	-3.23±1.06	24.37±5.42		1.13e-5±4.40e-7	348/358
			Band+BB	325.4±54.4	-0.91±0.20		24.55±5.20	-1.41	1.14e-5±4.40e-7	349/357
			CPL+BB+PL	294.6±24.3	-0.8		21.61±3.76	-1.5	1.15e-5±4.50e-7	350/359
			CPL _{-0.8} +BB+PL _{-1.5}	199.3±22.3	-0.79±0.09	-2.45±0.21			1.14e-5±4.30e-7	347/360
	22.147	22.343	Band	197.2±26.9	-0.65±0.25	-2.45±0.20	7.90±3.22	-1.57±1.16	8.39e-6±3.00e-7	346/358
			Band+BB	288.0±57.0	-0.99±0.41		26.04±7.30	-1.5	8.39e-6±3.10e-7	351/357
			CPL+BB+PL	236.7±21.2	-0.8		16.52±5.22		8.42e-6±3.60e-7	352/359
			CPL _{-0.8} +BB+PL _{-1.5}	125.6±14.4	-0.39±0.15	-2.16±0.09			8.21e-6±3.20e-7	379/360
	22.343	22.595	Band	325.0±45.0	-0.90±0.11	< -5	17.78±2.01		6.52e-6±2.30e-7	369/360
		Band+BB	321.5±48.2	-0.89±0.51		17.7±2.08	-1.60	6.75e-6±2.90e-7	369/357	
		CPL+BB+PL	304.8±30.7	-0.8		16.57±1.33	-1.51	6.73e-6±3.10e-7	370/359	
		CPL _{-0.8} +BB+PL _{-1.5}	239.0±58.3	-0.86±0.08	-2.29±0.17			6.69e-6±2.70e-7	396/360	
22.595	22.833	Band	279.2±30.0	-0.83±0.15	-2.32±0.21	13.94±4.17		7.68e-6±2.70e-7	392/358	
		Band+BB	328.3±45.6	-0.82±0.57		15.91±3.17	-1.59±0.58	7.68e-6±2.80e-7	401/357	
		CPL+BB+PL	313.8±31.8	-0.8		14.87±2.23	-1.5	7.70e-6±3.20e-7	402/359	
		CPL _{-0.8} +BB+PL _{-1.5}	286.2±30.0	-0.72±0.07	-2.47±0.22			7.65e-6±3.10e-7	366/360	
22.833	23.014	Band	391.2±60.4	-0.86±0.10	-3.22±0.99	26.93±9.30		1.13e-5±3.80e-7	366/358	
		Band+BB	409.3±56.9	-0.89±0.09		29.24±8.52	-0.82	1.16e-5±4.40e-7	365/357	
		CPL+BB+PL	261.7±26.9	-0.86±0.07	-2.65±0.32			1.17e-5±4.20e-7	430/360	
23.014	23.214	Band	370.4±54.1	-0.96±0.09	-3.75±2.69	19.85±3.57		9.42e-6±3.30e-7	421/358	
		Band+BB	370.5±53.1	-0.95±0.35		20.04±3.84	-1.74	9.67e-6±3.90e-7	421/357	
		CPL+BB+PL	329.9±28.2	-0.8		15.70±1.98	-1.5	9.68e-6±3.60e-7	427/359	
		CPL _{-0.8} +BB+PL _{-1.5}	246.1±28.5	-0.82±0.08	-2.35±0.17			9.60e-6±3.60e-7	384/360	
23.214	23.423	Band	262.1±28.5	-0.59±0.22	-2.41±0.20	10.62±1.82		9.21e-6±3.10e-7	378/358	
		Band+BB	306.1±36.5	-0.72±0.33		12.26±2.19	-1.40±0.66	9.25e-6±3.20e-7	391/357	
		CPL+BB+PL	324.3±29.1	-0.8		13.85±2.43	-1.5	9.25e-6±3.60e-7	382/359	
		CPL _{-0.8} +BB+PL _{-1.5}	313.3±26.7	-0.72±0.06	-2.90±0.42			9.34e-6±3.60e-7	400/360	
23.423	23.592	Band	329.8±34.2	-0.51±0.18	-2.98±0.47	13.05±2.22		1.27e-5±4.30e-7	393/358	
		Band+BB	347.9±32.6	-0.50±0.19		14.24±2.47	-1.33±1.16	1.27e-5±4.30e-7	393/358	
		CPL+BB+PL	510.3±40.9	-0.75±0.05	-3.24±0.62			1.28e-5±4.70e-7	416/360	
23.592	23.705	Band	510.3±56.0	-0.75±0.07	-3.28±0.67	25.04		2.39e-5±7.70e-7	416/358	
		Band+BB	450.7±48.3	-0.73±0.06	-2.33±0.14			2.39e-5±8.00e-7	361/360	
23.705	23.805	Band	470.0±66.8	-0.69±0.11	-2.36±0.15	16.57±8.78		2.53e-5±8.20e-7	360/358	
		Band+BB	409.9±39.5	-0.60±0.11	-2.28±0.12			2.54e-5±8.40e-7	345/360	
23.805	23.889	Band	562.4±100.0	-0.70±0.10	-2.42±0.17	31.00±7.41		2.84e-5±8.60e-7	340/358	
		Band+BB	310.1±30.8	-0.60±0.07	-2.26±0.12			2.88e-5±9.20e-7	343/360	
23.889	24.001	Band	523.5±88.4	-0.77±0.10	-2.58±0.26	25.79±3.87		2.21e-5±6.70e-7	332/358	
		Band+BB	597.0±67.0	-0.8		28.27±2.79	-1.5	2.28e-5±7.70e-7	334/359	
		CPL _{-0.8} +BB+PL _{-1.5}	266.7±30.7	-0.60±0.09	-2.11±0.09			2.30e-5±7.20e-7	382/360	
24.001	24.106	Band	306.6±48.3	-0.47±0.21	-2.18±0.11	13.45±3.09		2.07e-5±6.30e-7	377/358	
		Band+BB	488.1±67.0	-0.76±0.23		23.47±3.66	-1.36±0.42	2.09e-5±6.60e-7	380/357	
		CPL+BB+PL	541.9±56.1	-0.8		26.47±2.93	-1.5	2.16e-5±7.30e-7	381/359	
		CPL _{-0.8} +BB+PL _{-1.5}	313.9±27.5	-0.55±0.07	-2.46±0.17			2.17e-5±7.10e-7	366/360	
24.106	24.193	Band	662.3±84.6	-0.89±0.07	< -5	35.06±3.92		2.72e-5±8.30e-7	358/360	
		Band+BB	581.8±46.6	-0.8		30.96±3.10	-1.5	2.85e-5±8.90e-7	360/359	
		CPL _{-0.8} +BB+PL _{-1.5}	293.2±35.9	-0.78±0.07	-2.18±0.11			2.23e-5±2.23e-5	363/360	
24.193	24.290	Band	440.8±94.8	-0.91±0.10	-2.37±0.20	23.03±6.17		2.13e-5±6.60e-7	361/358	
		Band+BB	538.7±88.5	-0.99±0.10		26.49±4.84	-1.27±0.57	2.18e-5±7.50e-7	361/357	
		CPL+BB+PL	464.8±44.9	-0.8		22.10±3.10	-1.5	2.23e-5±7.30e-7	362/359	
		CPL _{-0.8} +BB+PL _{-1.5}	274.3±21.2	-0.62±0.07	-2.92±0.35			2.23e-5±7.50e-7	347/360	
24.290	24.390	Band	266.9±24.4	-0.38±0.25	-2.86±0.31	9.72±2.03		1.94e-5±6.40e-7	345/358	
		Band+BB	317.5±35.3	-0.69±0.14		25.14±10.60	-1.29±1.25	1.94e-5±6.30e-7	347/357	
		CPL+BB+PL	208.1±22.9	-0.59±0.09	-2.25±0.12			1.96e-5±6.90e-7	361/360	
24.390	24.510	Band	208.8±37.0	-0.59±0.19	-2.25±0.12	12.21		1.55e-5±4.90e-7	361/358	

GRB	T-start (s)	T-end (s)	模型	Band/CPL			BB	PL	$F_p/\text{keV s}^{-1} \text{cm}^{-2}$	Cstat/DOF
				E_p/keV	α	β	kT/keV	p		
151231443	24.793	24.965	Band	170.7±20.4	-0.59±0.11	-2.17±0.10			1.14e-5±4.40e-7	368/360
			Band+BB	180.3±29.3	-0.24±0.44	-2.21±0.11	9.37±1.77		1.01e-5±3.40e-7	363/358
			CPL+BB+PL	276.6±36.5	-0.69±0.50		17.17±3.32	-1.48±0.44	1.02e-5±3.40e-7	371/357
	24.965	25.167	Band	301.9±30.6	-0.8		19.83±2.45	-1.5	1.00e-5±4.00e-7	371/359
			CPL _{0.8} +BB+PL _{1.5}	218.6±24.4	-0.86±0.08	-2.60±0.27			1.02e-5±3.90e-7	396/360
			Band	234.4±30.0	-0.46±0.30	-2.64±0.30	9.93±1.10		8.21e-6±3.00e-7	384/358
	25.167	25.455	Band+BB	289.8±27.5	-0.81±0.15		12.37±1.86	-1.21	8.24e-6±3.00e-7	386/357
			CPL+BB+PL	293.7±25.5	-0.8		11.83±1.41	-1.5	8.35e-6±3.40e-7	385/359
			CPL _{0.8} +BB+PL _{1.5}	143.5±19.1	-0.84±0.11	-2.34±0.16			8.37e-6±3.40e-7	406/360
	25.455	25.832	Band	365.0±110.0	-1.37±0.11	< -5	25.83±2.83		5.14e-6±3.10e-7	409/358
			Band+BB	354.2±138.0	-1.37±0.12		25.88±2.85	-1.10	5.29e-6±2.30e-7	409/357
			CPL+BB+PL	152.8±103.6	-0.8		23.35	-1.5	5.27e-6±2.40e-7	415/359
	25.832	26.307	CPL _{0.8} +BB+PL _{1.5}	109.7±13.1	-0.64±0.14	-2.24±0.11			4.83e-6±1.90e-7	328/360
			Band	229.9±21.8	-0.76±0.18	< -5	10.66±0.99		4.23e-6±1.70e-7	314/358
			Band+BB	252.1±42.3	-1.00±0.56		13.03±1.61	-1.57	4.19e-6±1.90e-7	317/357
	26.307	26.949	CPL+BB+PL	230.9±22.7	-0.8		11.36±1.96	-1.5	4.31e-6±1.90e-7	314/359
			CPL _{0.8} +BB+PL _{1.5}	118.8±13.1	-0.71±0.13	-2.46±0.19			4.24e-6±1.90e-7	382/360
			Band	141.4±20.8	-0.39±0.41	-2.62±0.29	8.63±1.47		3.05e-6±1.40e-7	377/358
	26.949	28.153	Band+BB	161.1±18.1	-0.8		11.36±1.96	-1.5	3.02e-6±1.40e-7	383/359
			CPL _{0.8} +BB+PL _{1.5}	101.4±15.4	-0.80±0.16	-2.16±0.11			2.90e-6±1.37e-7	377/360
			Band	104.1±22.0	-0.01±1.17	-2.18±0.17	6.28±0.85		2.46e-6±1.10e-7	374/358
	28.153	35.136	Band+BB	127.3±10.9	-1.10±0.08	< -5			2.45e-6±1.10e-7	427/360
			Band	203.6±71.6	-1.18±0.58		11.36±1.96	-1.57±0.90	1.21e-6±5.80e-8	383/359
			CPL+BB+PL	53.65±11.5	-0.71±0.38	-2.23±0.16			2.90e-6±1.30e-7	473/360
	35.136	3.478	Band	135.4±23.8	-1.30±0.14	-2.48±0.25			2.56e-7±2.20e-8	392/360
			Band+BB	162.1±29.5	-0.71±2.48	-2.56±0.25	9.38±1.07		1.12e-6±4.20e-8	374/358
			CPL+BB+PL	186.4±19.7	-1.32±0.35		9.50±1.32	-1.69±0.42	1.10e-6±4.00e-8	377/357
	3.478	5.006	CPL _{0.7} +BB+PL _{1.5}	192.7±21.9	-0.7		9.35±0.75	-1.5	1.07e-6±4.30e-8	378/359
			Band	217.0±17.1	-0.84±0.09	-2.79±0.27			1.07e-6±3.80e-8	434/360
			Band+BB	226.3±21.5	-0.13±0.65	-0.77±0.23	12.10±1.21		4.29e-6±1.10e-7	423/358
	5.006	5.884	Band+BB	293.2±39.8	-0.89±0.53		18.87±3.47	-1.88	4.27e-6±1.10e-7	427/357
			CPL+BB+PL	516.6±46.0	-0.7		14.83±1.71	-1.5	4.29e-6±1.00e-6	428/359
			CPL _{0.7} +BB+PL _{1.5}	379.3±30.7	-0.84±0.07	-2.71±0.25			4.30e-6±1.40e-7	354/360
	5.884	6.778	Band	500.1±51.0	-0.78±0.12	-3.20±0.64	24.83±3.32		8.78e-6±2.10e-7	338/358
			Band+BB	419.9±26.1	-0.7		25.40±3.21	-1.5	8.90e-6±2.20e-7	339/358
			CPL _{0.7} +BB+PL _{1.5}	381.8±31.3	-0.85±0.07	-2.69±0.25			8.95e-6±2.00e-7	415/360
	6.778	7.840	Band	501.3±57.8	-0.83±0.11	-3.05±0.54	27.22±4.18		8.02e-6±1.90e-7	400/358
			Band+BB	417.6±28.3	-0.7		27.54±3.92	-1.5	8.10e-6±2.00e-7	406/359
			CPL _{0.7} +BB+PL _{1.5}	333.3±30.7	-0.98±0.07	-2.73±0.31			8.24e-6±1.90e-7	376/360
	7.840	12.128	Band	366.3±39.5	-0.86±0.16	-2.87±0.41	15.85±3.69		6.43e-6±1.60e-7	372/358
			Band+BB	442.5±53.2	-1.08±0.08		29.83±7.07	-0.16±5.55	6.44e-6±1.70e-7	378/359
			CPL+BB+PL	370.7±26.5	-0.7		15.05±1.84	-1.5	6.54e-6±1.70e-7	376/359
	12.128	64.167	CPL _{0.7} +BB+PL _{1.5}	200.1±21.8	-0.71±0.13	-2.34±0.13			6.47e-6±1.60e-7	473/360
			Band	273.4±79.6	-0.89±0.24	-2.51±0.17	24.64±8.26		2.15e-6±5.70e-8	471/358
			Band+BB	364.4±43.3	-0.84±0.31		24.53±6.96	-1.43±0.39	2.15e-6±5.90e-8	467/359
	64.167	65.754	CPL+BB+PL	253.1±28.2	-0.7		22.64±4.02	-1.5	2.11e-6±6.70e-8	467/359
			CPL _{0.7} +BB+PL _{1.5}	179.7±27.4	-1.15±0.14	-2.84±0.68			2.10e-6±5.80e-8	458/360
			Band	78.0±79.1	-1.38±0.61	-2.11±0.28	47.27±7.76		3.01e-7±1.50e-8	455/358
	65.754	67.928	Band+BB	56.63±72.9	-0.81±2.71		50.76±17.4	-1.94±0.11	2.99e-7±1.40e-8	454/357
			CPL+BB+PL	167.1±18.5	-0.7		6.19±2.04	-1.5	2.93e-7±1.60e-8	456/359
			CPL _{0.7} +BB+PL _{1.5}	219.7±20.8	-0.84±0.10	-2.53±0.18			2.90e-7±1.20e-8	360/361
	67.928	69.925	Band	314.8±65.1	-1.08±0.15	-2.91±0.63	30.04±6.94		4.21e-6±1.10e-7	358/358
			Band+BB	302.9±46.0	-1.08±0.13		30.81±6.81	0.50±1.96	4.24e-6±1.20e-7	353/357
			CPL+BB+PL	246.7±23.2	-1.5		19.75±4.10	-1.5	4.16e-6±1.50e-7	361/359
69.925	71.452	CPL _{0.7} +BB+PL _{1.5}	219.8±15.9	-0.90±0.09	-3.30±0.70			4.11e-6±1.10e-7	403/360	
		Band	223.9±17.3	-0.54±0.37	-3.21±0.52	10.30±1.77		3.05e-6±8.90e-8	400/358	
		Band+BB	223.1±16.8	-0.89±0.09		10.42±1.85	-1.34±0.63	3.03e-6±9.00e-8	399/357	
71.452	90.624	CPL+BB+PL	222.5±16.4	-0.7		10.59±2.98	-1.5	2.98e-6±9.20e-8	399/359	
		CPL _{0.7} +BB+PL _{1.5}	134.6±10.7	-0.34±0.17	-2.75±0.18			3.01e-6±8.50e-8	426/360	
		Band	167.6±58.0	-0.64±0.55	-2.87±0.33	23.30±8.75		2.87e-6±8.70e-8	426/358	
90.624	90.624	Band+BB	144.8±7.45	-0.55±0.79		22.41±7.21	-1.65±0.50	2.86e-6±9.00e-8	426/357	
		CPL+BB+PL	180.3±18.3	-0.7		24.17±3.04	-1.5	2.79e-6±9.10e-8	427/359	
		CPL _{0.7} +BB+PL _{1.5}	164.8±9.38	-0.59±0.11	-3.36±0.45			2.79e-6±8.10e-8	392/60	
90.624	90.624	Band	186.4±14.9	-0.11±0.56	-3.44±0.52	13.44±1.96		3.63e-6±1.10e-7	387/358	
		Band+BB	197.3±25.2	-0.05±1.06		15.08±2.71	-1.88±0.46	3.60e-6±1.10e-7	388/357	
		CPL+BB+PL	198.7±17.1	-0.7		18.69±3.02	-1.5	3.55e-6±1.00e-7	390/359	
90.624	90.624	CPL _{0.7} +BB+PL _{1.5}	81.4±11.9	-0.02±0.51	-2.34±0.12			3.63e-6±1.10e-7	394/360	
		Band	131.3±43.5	0.39±3.62	-2.47±0.25	11.63±2.94		4.58e-7±2.20e-8	392/358	
		Band+BB	142.1±47.4	0.31±3.42		13.06±2.56	-1.60±0.32	4.53e-7±2.30e-8	394/357	
90.624	90.624	CPL+BB+PL	140.3±29.8	-0.7		15.23±2.36	-1.5	4.39e-7±2.60e-8	394/359	

5. Discussion and conclusions

According to the time-integrated and time-resolved analysis results, the spectra can be modeled with a combination of non-thermal component (Band/CPL) and thermal component (BB), and the extra power law component can be modeled in the low-energy band (see Sec.4). In a standard fireball model, that the spectra should be thermal, which is inconsistent with observations. In this section, we mainly discuss the fitting results and spectral evolution of Band+BB.

5.1 the low-energy index α

The value of α slightly softens when adding a BB to the Band for most GRBs, but the scenario does not occur of the value of β (see Figures 3 and 4). In other words, the thermal component mainly affect the low-energy spectra and the effect of the high-energy range is not obvious in GRBs time-resolved spectra. In addition, the value is less than $-2/3$ and $-3/2$ of low-energy power-law index α of empirical Band function which correspond to the slow- and fast-cooling synchrotron radiation, respectively (Sari et al. 1998). And the radiative electron will be accelerated to relativistic velocity due to the collision in the internal shock model, so that the α are not beyond $-2/3$ because relativistic electron will fast cool after the collision (Katz 1994). In our fitting results, there are only four bursts satisfied with the internal-shock synchrotron radiation.

For GRB121225417, all the values of α are less than $-2/3$ and vary between -1.5 and -1 in our fitting results. It implies that GRB121225417 agrees well with fast-cooling synchrotron radiation; For GRB130518580, except the time interval 26.714 ~ 27.277 s, the values of α vary from -0.64 to -1, which can be regarded as slow-cooling synchrotron radiation; For GRB151227218, except the time interval 30.219 ~ 30.624 s, the values of α are closed to or less than -1, which is similar to GRB121225417; For GRB160422499, the variation range of α is large than others, but the value is cluster in -1.1 which is satisfied with fast-cooling synchrotron radiation.

In the other hand, the radiative efficiency of internal shock model is too less according to observation (Boucher et al. 2009). Some study shows the efficiency can increase through the continuous collision after the first accelerating (Spada et al. 2001), or if there are about 1/2 prompt emission radiation rooting in the thermal radiation, the low-efficiency non-thermal radiation will occur.

To deal with the problems in the internal shock model, one way is that perhaps the γ photons are produced by other radiative mechanisms. If the electron's transverse deflections are much less than the beaming angle in a random and small-scale magnetic fields, the radiative mechanism is not synchrotron radiation but jitter radiation (Medvedev 2000). Medvedev (2006) presented that the value of α ranging from 0 to -1 of jitter radiation depend on the angle of line-of-sight. This model can naturally explain the typical value, $\alpha=-1$, of GRB observations and predicts that about a quarter of time-resolved spectra should have hard values of α , which violates the synchrotron line of death. In our fitting results, there are just three bursts agree well with the jitter radiation, we showed it in Figure 7, and the ratio beyond $-2/3$ is 23.08%, 21.98%, 21.95% of GRB120707800, GRB150627183, GRB150201574, respectively. However, the small-scale magnetic field assumed in the jitter radiation actually could not be reproduce from relativistic shocks in numerical simulations (Sironi & Spitkovsky 2009), which indicates that jitter radiation is not a credible candidate of radiative mechanism in GRB prompt emission. Except for the mechanism we have mentioned above, the self-synchrotron radiation (SSC) is always used to explain the γ photons emission.

However, the synchrotron radiation seems remain a better model to explain a large proportion of the prompt emission, so that sometimes we must give up the internal shock model. If in the Collision-Induced Magnetic Reconnection and Turbulence (ICMRAT) model the magnetic field is strong enough, the radiative electrons will be accelerated by the reconnection until it ends (Narayan & Kumar 2009), and the deadline of internal shock fast-cooling synchrotron radiation can be avoided. Besides, the simulation of ICMRT model pointed out that there are two components in the instantaneous radiation light curve: the slow component produced by the reconnection event and the fast component produced by the shell collision, and the observations have also confirmed the theoretical prediction (Gao & Zhang 2012).

5.2 the $E_p - kT$ relation

The jet component of prompt emission has been discussed in several decades, and it can be divided into two classes, matter-dominant and magnetic-dominant. Burgess et al. (2014b) showed there are a linear correlation between the characteristic parameters of non-thermal and thermal component, the peak energy E_p and the thermal temperature T , $E_p \propto T^\delta$, and the value of δ can be interpreted by the jet which is dominated by magnetic or kinetic energy, which is equal to $6(3\mu - 1)/(14\mu - 5)$ and 1.2, respectively, where μ depends on the bulk Lorentz factor on the radius, $\Gamma \propto R^\mu$. We showed our results in Table 5 and the eight burst correlations have presented in Figure 8. The value of δ is between 0 and 0.8. We can get that μ floats around 0.31 by $6(3\mu-1)/(14\mu-1)=\delta$ and the values of μ for each burst indicated that the jet is magnetic-dominant. Therefore, in the Band(+BB) model, the δ of magnetic-dominant jet is about 0.5. We make sure the jet component through the $E_p - kT$ relation. Similar scenario has been found in

GRB080916C. It has been suggested that there is a magnetically dominated outflow entrained with baryonic matters, which indicates that the thermal component is weak in a Poynting flux (Zhang & Pe'er 2009). However, Guiriec et al. (2015a) pointed out that the thermal component can be modeled with a multi-component model CPL+BB+PL in the time-resolved spectra. Additionally, a hybrid jet is composed of thermal (hot fireball) component and non-thermal (cold Poynting flux) component if the fireball expands first thermally and then magnetically and with such a hybrid jet the mechanism is likely Internal Collision-Induced Magnetic Reconnection and Turbulence (ICMRAT) to power the non-thermal emission (Gao & Zhang 2015). From Table 5 there is a significant thermal component in the time-resolved spectra of the eight bursts, which implies that there are hybrid jets in most GRBs.

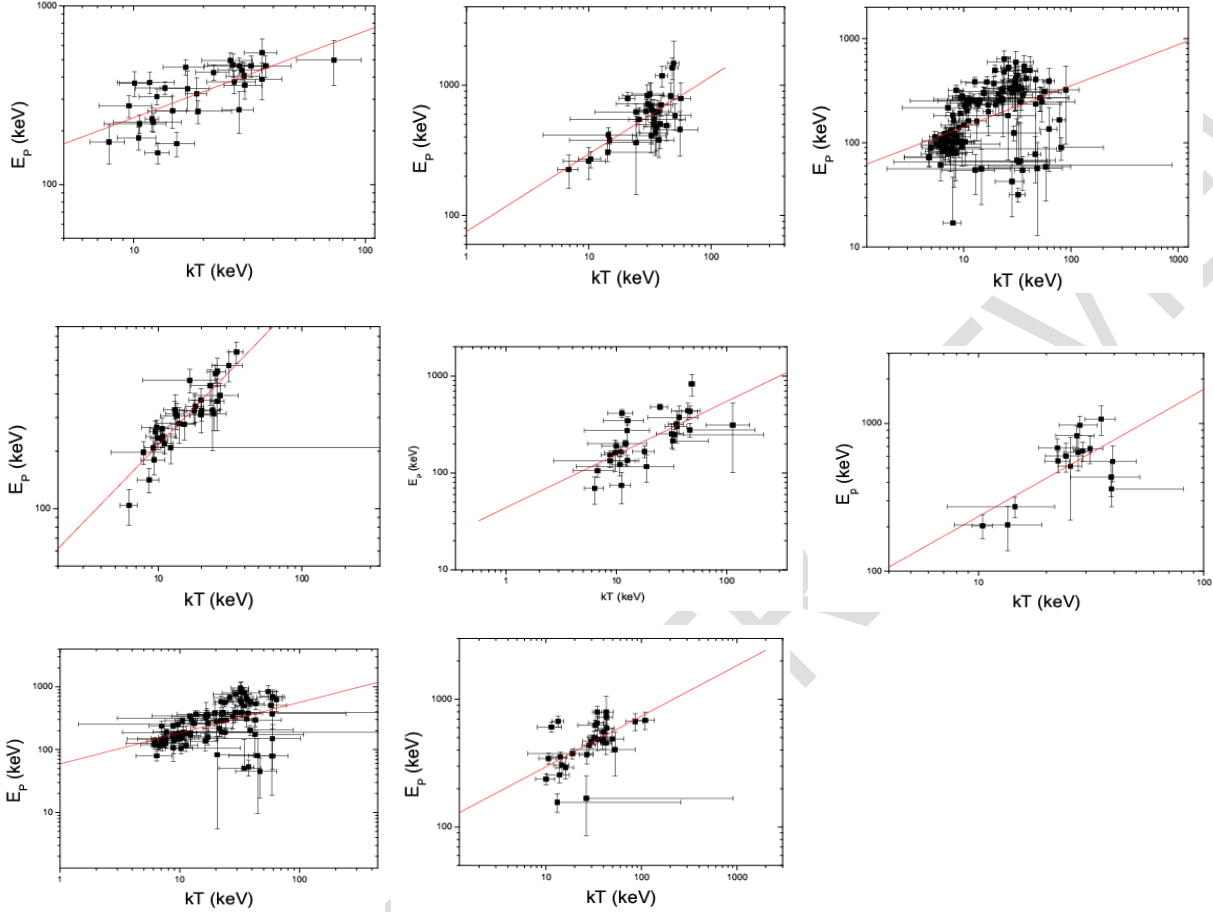


Fig. 8 E_p - kT correlation. The red line is the best fitting line of the data.

Table 5 Fitting results of E_p - kT linear relationship under Band+BB model

GRB	δ	μ	r	P
100724029	0.53 ± 0.10	0.318 ± 0.01	0.7615	$< 1 \times 10^{-4}$
120129580	0.49 ± 0.09	0.282 ± 0.01	0.7062	$< 1 \times 10^{-4}$
120707800	0.27 ± 0.37	—	-0.2188	0.4727
121225417	0.50 ± 0.50	—	0.2665	0.2852
130305486	-0.18 ± 0.17	—	-0.4005	0.3255
130502327	0.17 ± 0.16	—	0.2356	0.2791
130504978	0.11 ± 0.12	—	0.1310	0.3911
130518580	0.59 ± 0.11	0.313 ± 0.01	0.6901	$< 1 \times 10^{-4}$
130606497	0.23 ± 0.11	—	0.2332	0.0339
131231198	0.39 ± 0.08	0.323 ± 0.01	0.4184	$< 1 \times 10^{-4}$
140206275	0.80 ± 0.48	—	0.4187	0.1203

140329295	0.78±0.07	0.297±0.01	0.8890	< 1×10 ⁻⁴
140523129	0.55±0.11	0.308±0.02	0.6870	< 1×10 ⁻⁴
150201574	0.27±0.10	–	0.3522	0.0131
150314205	0.47±0.28	–	0.2707	0.1103
150403913	0.86±0.25	0.320±0.08	0.6743	0.0042
150627183	0.49±0.10	0.285±0.01	0.4764	< 1×10 ⁻⁴
150902733	0.40±0.11	0.319±0.01	0.5715	0.0009
151227218	0.11±0.25	–	0.1049	0.6788
151231443	0.06±0.34	–	0.0519	0.8728
160422499	-0.03±0.02	–	-0.0021	0.9883

From left to right are the names of GRBs, δ : Ep-kT linear relationship index; parameters μ ; r: linear correlation coefficient; P: confidence level.

UNDER PEER REVIEW

5.3 The $E_p - F_p$ relation

Most study shows that there is a linear relation between the rest frame peak energy $E_{p,z}$ and isotropic luminosity L_{iso} , $L_{iso} \propto E^k$, where k is the power law index (Yonetoku et al. 2004, Lu et al. 2012). The parameter $E_{p,z}$ ($E_p(1+z)$) and L_{iso} ($4\pi d_L^2 F_p$) can be measured by the redshift and the parameters of observations, where d_L is the luminosity distance in units of cm ; F_p is the peak flux of νF_ν spectra in units of $keV s^{-1} cm^{-2}$; z is the redshift.

Therefore, we presented the linear relation, $F_p \propto E_p^k$ of the 20 bursts in Table 6. The linear correlation of Band Only is better than those in Band+BB, and the value of k is between 0 to 2. Besides, the average value of k is +1.45 in Band Only which is close to the results presented by Guiriec et al. (2013), which seems to be intrinsic in the time-resolved spectra of GRB. However, fitting to the data with Band+BB does not lead to the linear correlation. Guiriec et al. (2015a) have proposed that if the additional component of the spectra is very intense, it will lead to large scatters in a weaker and biased relation or even no correlation at all. From Table 6, the significant thermal component contribution in the prompt emission spectra of the 20 bursts might bring about the weak correlation.

Table 6 The E_p - F_p relationship in two different models

GRB	model	k	r	P
100724029	Band	1.44 ± 0.23	0.8057	$<1 \times 10^{-4}$
	Band+BB	0.29 ± 0.19	0.2110	0.1257
120129580	Band	1.94 ± 0.26	0.8092	$<1 \times 10^{-4}$
	Band+BB	2.37 ± 0.27	0.8502	$<1 \times 10^{-4}$
120707800	Band	1.47 ± 0.25	0.8746	$<1 \times 10^{-4}$
	Band+BB	0.92 ± 0.27	0.7138	0.0061
121225417	Band	1.06 ± 0.20	0.7841	$<1 \times 10^{-4}$
	Band+BB	0.54 ± 0.17	0.6326	0.0049
130305486	Band	2.95 ± 2.53	0.4299	0.2878
	Band+BB	None		
130502327	Band	0.84 ± 0.25	0.436	0.0017
	Band+BB	1.45 ± 0.60	0.3341	0.0203
130504978	Band	1.30 ± 0.16	0.7695	$<1 \times 10^{-4}$
	Band+BB	0.86 ± 0.18	0.5861	$<1 \times 10^{-4}$
130518580	Band	2.06 ± 0.51	0.5801	0.0003
	Band+BB	1.38 ± 0.38	0.5410	0.0009
130606497	Band	0.84 ± 0.05	0.8695	$<1 \times 10^{-4}$
	Band+BB	0.75 ± 0.07	0.7777	$<1 \times 10^{-4}$
131231198	Band	0.72 ± 0.08	0.6290	$<1 \times 10^{-4}$
	Band+BB	0.58 ± 0.08	0.5459	$<1 \times 10^{-4}$
140206275	Band	1.04 ± 0.43	0.5714	0.0328
	Band+BB	0.59 ± 0.25	0.5576	0.0383
140329295	Band	1.89 ± 0.31	0.7247	$<1 \times 10^{-4}$
	Band+BB	1.09 ± 0.38	0.4593	0.0072
140523129	Band	1.11 ± 0.18	0.7531	$<1 \times 10^{-4}$
	Band+BB	0.97 ± 0.25	0.6044	0.0007
150201574	Band	1.91 ± 0.18	0.8189	$<1 \times 10^{-4}$
	Band+BB	1.23 ± 0.24	0.6013	$<1 \times 10^{-4}$
150403913	Band	1.47 ± 0.28	0.7940	$<1 \times 10^{-4}$
	Band+BB	0.47 ± 0.39	0.3079	0.2461
150627183	Band	1.00 ± 0.11	0.6773	$<1 \times 10^{-4}$
	Band+BB	0.72 ± 0.11	0.5707	$<1 \times 10^{-4}$
150902733	Band	1.48 ± 0.26	0.7314	$<1 \times 10^{-4}$
	Band+BB	1.44 ± 0.39	0.5743	0.0009
151227218	Band	1.44 ± 0.24	0.8275	$<1 \times 10^{-4}$
	Band+BB	0.86 ± 0.38	0.4923	0.0380

151231442	Band	2.22 ± 0.52	0.8043	0.0016
	Band+BB	1.78 ± 0.26	0.9071	$< 1 \times 10^{-4}$
160422499	Band	1.40 ± 0.10	0.8868	$< 1 \times 10^{-4}$
	Band+BB	1.29 ± 0.10	0.8811	$< 1 \times 10^{-4}$

Among the 20 selected bursts, we only know the redshift of GRB150403029. The luminosity distance d_L can be calculated by the redshift. And we can determine the corresponding isotropic luminosity L_{iso} and the peak energy $E_{p,z}$ in the rest frame. Then we can make its linear relationship. The correlation between the isotropic luminosity L_{iso} and the peak energy $E_{p,z}$ in rest frame when the time-resolved data is fitted with two different models. We showed it in Figure 9. The results showed that the BB component will change the correlation of the isotropic luminosity L_{iso} and the peak energy $E_{p,z}$. In the early research work, Liang et al. (2004) pointed out that in the 2048 GRB time-resolved spectra observed by BATSE, the similar results to Yonetoku were obtained. After defining a parameter ω that related to the redshift, and limiting the parameters of the fireball without correlation, the internal shock wave model and the external shock model in the fireball can better explain this linear relationship and the values of the parameter ω . However, it requires a higher requirement for the fireball. Some studies indicate that if the prompt radiation process of the GRBs satisfies the synchrotron radiation mechanism, there will be a linear relationship similar to that in the synchrotron luminosity L_{syn} and the Doppler factor D , $L_{syn} \propto D^{3.1}$. After the Doppler factor and redshift were corrected, there is a similar $E_{p,z}$ - L_{iso} relationship between them. The case indicating that the jet between the Gamma-ray bursts and the blazar is likely to come from the same radiation process. At the radiation spectrum 5GHZ, there is a similar linear relationship between luminosity L_ν and v_{peak} , the radio-X-ray wave composite spectrum index α_{RX} of GRBs and the active galactic nucleus, that is, the radiation process satisfies the synchronous accelerated radiation.

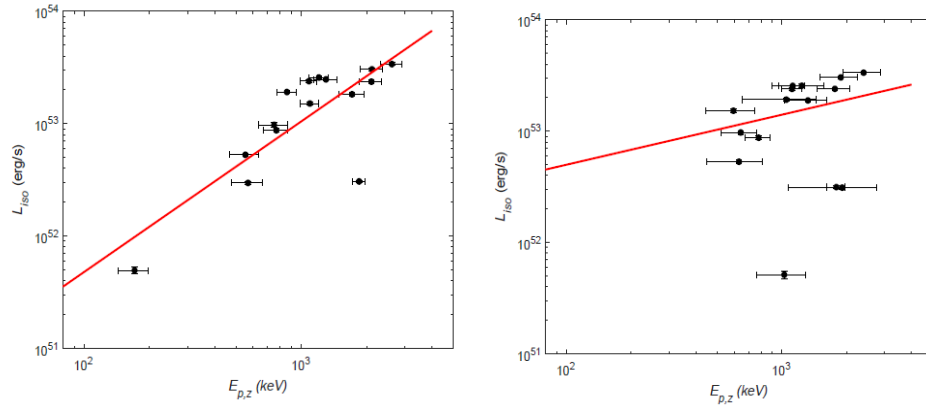


Fig. 9 The correlation between the isotropic luminosity L_{iso} and the peak energy $E_{p,z}$ of GRB 150403913 when the time-resolved data is fitted with two different models. Left panels: relationship of $E_{p,z}$ - L_{iso} , Spearman correlation coefficient $r = 0.81$ and the chance probability $P < 0.0001$ in Band model. Right panels: $E_{p,z}$ - L_{iso} Spearman correlation coefficient $r = 0.38$ and the chance probability $P = 0.1607$ in Band+BB model.

5.4 the spectral component

General speaking, the spectra of GRB prompt emission can be fitted with thermal and non-thermal component. We will discuss the origin of each component from the sub-photosphere emission and photosphere emission. If the energy dissipates below or closed to the photosphere, the electron will be accelerated by the dissipative process, the γ photons will be produced by synchrotron radiation at low-energy band, i.e. keV \sim MeV band (Rees & Mészáros 2005; Chhotray & Lazzati 2015), and the Comptonized process at high-energy band. Such a mechanism will lead to a single complex shape than Band or CPL. That is the spectra cannot be fitted with multi-component model. In the other hand, the electron surrounding the source will be accelerated by the dissipative energy from the fireball. Subsequently, the high-energy electron distribution will be in quasi-static under the combined action of the acceleration by external shock and the IC process, and the temperature will be greater than that of the photosphere (Pe'er 2013).

If there is no energy dissipation below the photosphere or the dissipation do not significantly affected the photosphere, the special geometry of the photosphere remains thermal (Lundman et al. 2013; Pe'er 2008). In this scenario, the non-thermal component might be produced by the optically thin synchrotron radiation, the emission electrons would be accelerated by internal shock (Rees & Mészáros 1994; Sari et al. 1998) and magnetic reconnection (Zhang & Yan 2011). The extra PL component can be modeled in multi-component model in early stage of the prompt emission, which indicates the physical

origin of this component is in internal origin instead of the external shock, and the PL photons might be produced by the Compton scattering in Thomson regime (Guiriec et al. 2015a).

CONSENT (WHERE EVER APPLICABLE)

All authors declare that 'written informed consent was obtained from the patient (or other approved parties) for publication of this case report and accompanying images'.

ETHICAL APPROVAL (WHERE EVER APPLICABLE)

This study is not against the public interest, or that the release of information is allowed by legislation.

REFERENCES

1. Band D, Matteson J, Ford L, Schaefer B, Palmer D, Teegarden B, et al. BATSE Observations of Gamma-Ray Burst Spectra. I. Spectral Diversity. 1993, *The Astrophysical Journal*, 413, 281-292, [10.1086/172995](https://doi.org/10.1086/172995).
2. Bhat P, Guiriec S. An overview of the current understanding of Gamma Ray Bursts in the Fermi era. *Bulletin of the Astronomical Society of India*, 2011; 39(3), 471-515
3. Burgess J M. On spectral evolution and temporal binning in gamma-ray bursts. *Monthly Notices of the Royal Astronomical Society*, 2014, 445(3), 2589-2598. [10.1093/mnras/stu1925](https://doi.org/10.1093/mnras/stu1925).
4. Burgess J M, Preece R D, Ryde F, Veres P, Mészáros P, Connaughton V, et al. An Observed Correlation between Thermal and Non-thermal Emission in Gamma-Ray Bursts. *The Astrophysical Journal Letters*, 2014b, 784(2), L43-L47. [10.1088/2041-8205/784/2/L43](https://doi.org/10.1088/2041-8205/784/2/L43).
5. Crider A, Liang E P, Smith I A, Preece R D, Briggs M S, Pendleton G N, et al. Evolution of the Low-Energy Photon Spectral in Gamma-Ray Bursts. *The Astrophysical Journal*, 1997, 479, L39 -L42. [10.1086/310574](https://doi.org/10.1086/310574).
6. Chhotray A, Lazzati D. Gamma-ray Burst Spectra and Spectral Correlations from Sub-photospheric Comptonization. *The Astrophysical Journal*, 2015, 802(2), 132-142. [10.1088/0004-637X/802/2/132](https://doi.org/10.1088/0004-637X/802/2/132).
7. Daigne F, Mochkovitch R. The Expected Thermal Precursors of Gamma-Ray Bursts in the Internal Shock Model. *AIP Conference Proceedings*, 2003, 662, 289-291. [10.1063/1.1579361](https://doi.org/10.1063/1.1579361).
8. Fryer C L, Woosley S E, Hartmann D H. Formation Rates of Black Hole Accretion Disk Gamma-Ray Bursts. *The Astrophysical Journal*, 1999, 526(1), 152-177. [10.1086/307992](https://doi.org/10.1086/307992).
9. Goodman J. Are gamma-ray bursts optically thick? *Astrophysical Journal*, 1986, 308, L47-L50. [10.1086/184741](https://doi.org/10.1086/184741).
10. Guiriec S, Connaughton V, Briggs M S, Burgess M, Ryde F, Daigne F, et al. Detection of a Thermal Spectral Component in the Prompt Emission of GRB 100724B. *The Astrophysical Journal*, 2011, 727(2), L33-L37. [10.1088/2041-8205/727/2/L33](https://doi.org/10.1088/2041-8205/727/2/L33).
11. Guiriec S, Daigne F, Hascoët R, Vianello G, Ryde F, Mochkovitch R, et al. Evidence for a Photospheric Component in the Prompt Emission of the Short GRB 120323A and Its Effects on the GRB Hardness-Luminosity Relation. *The Astrophysical Journal*, 2013, 770(1), 32-57. [10.1088/0004-637X/770/1/32](https://doi.org/10.1088/0004-637X/770/1/32).
12. Guiriec S, Kouveliotou C, Daigne F, Zhang B, Hascoët R, Nemmen R S, et al. Toward a Better Understanding of the GRB Phenomenon: a New Model for GRB Prompt Emission and its Effects on the New $L_i^{NT} - E_{peak,i}^{rest,NT}$ Relation. *The Astrophysical Journal*, 2015a, 807(2), 148-202. [10.1088/0004-637X/807/2/148](https://doi.org/10.1088/0004-637X/807/2/148).
13. Guiriec S, Mochkovitch R, Piran T, Daigne F, Kouveliotou, C.; Racusin, J., et al. GRB 131014A: A Laboratory for Studying the Thermal-like and Non-thermal Emissions in Gamma-Ray Bursts, and the New $L_i^{nTh} - E_{peak,i}^{nTh,rest}$ Relation. *The Astrophysical Journal*, 2015b, 814(1), 10-35. [10.1088/0004-637X/814/1/10](https://doi.org/10.1088/0004-637X/814/1/10).
14. Gao H, Zhang B.-B, Zhang B, Stepwise Filter Correlation Method and Evidence of Superposed Variability Components in Gamma-Ray Burst Prompt Emission Light Curves. *The Astrophysical Journal*, 2012, 748(2), 134-148. [10.1088/0004-637X/748/2/134](https://doi.org/10.1088/0004-637X/748/2/134).

15. Huang S, Yin Y, Peng Z.-Y. Investigating the thermal component in GRB100724B. *Astrophysics and Space Science*, 2016, 361, 362-371. [10.1007/s10509-016-2937-3](https://doi.org/10.1007/s10509-016-2937-3).
16. Katz J I. Low-Frequency Spectra of Gamma-Ray Bursts. *The Astrophysical Journal*, 1994, 432, L107-L109. [10.1086/187523](https://doi.org/10.1086/187523).
17. Lundman C, Pe'er A, Ryde F. A theory of photospheric emission from relativistic, collimated outflows. *Monthly Notices of the Royal Astronomical Society*, 2013, 428, 2430-2442. [10.1093/mnras/sts219](https://doi.org/10.1093/mnras/sts219).
18. Liang E W, Dai Z G, Wu X F. The Luminosity- E_p Relation within Gamma-Ray Bursts and the Implications for Fireball Models. *The Astrophysical Journal*, 2004, 606, L29-L32. [10.1086/421047](https://doi.org/10.1086/421047).
19. MacFadyen A I, Woosley S E. Collapsars: Gamma-Ray Bursts and Explosions in "Failed Supernovae". *The Astrophysical Journal*, 1999, 524, 262-289. [10.1086/307790](https://doi.org/10.1086/307790).
20. Medvedev M V. Theory of "Jitter" Radiation from Small-Scale Random Magnetic Fields and Prompt Emission from Gamma-Ray Burst Shocks. *The Astrophysical Journal*, 2000, 540, 704-714. [10.1086/309374](https://doi.org/10.1086/309374).
21. Medvedev M V. The Theory of Spectral Evolution of the Gamma-Ray Burst Prompt Emission. *The Astrophysical Journal*, 2006, 637, 869-872. [10.1086/498697](https://doi.org/10.1086/498697).
22. Meegan C A, Fishman G J, Wilson R B, Paciesas W. S, Brock M N, Horack J M, et al. Gamma-Ray Bursts. 1992, IAU Circ, 5641.
23. Meegan C, Lichti G, Bhat P N, Bissaldi E, Briggs M S, Connaughton V, et al. The Fermi Gamma-ray Burst Monitor. *The Astrophysical Journal*, 2009, 702, 791-804. [10.1088/0004-637X/702/1/791](https://doi.org/10.1088/0004-637X/702/1/791).
24. Mészáros P, Rees M J. Gamma-Ray Bursts: Multiwaveband Spectral Predictions for Blast Wave Models. *The Astrophysical Journal*, 1993, 418, L59-L62. [10.1086/187116](https://doi.org/10.1086/187116).
25. Narayan R, Kumar P. A turbulent model of gamma-ray burst variability. 2009, MNRAS, 394, L117-L120. [10.1111/j.1745-3933.2009.00624.x](https://doi.org/10.1111/j.1745-3933.2009.00624.x).
26. Paczynski B. Gamma-ray bursters at cosmological distances. *The Astrophysical Journal*, 1986, 308, L43-L46. [10.1086/184740](https://doi.org/10.1086/184740).
27. Pe'er A. Temporal Evolution of Thermal Emission from Relativistically Expanding Plasma. *The Astrophysical Journal*, 2008, 682(1), 463-473. [10.1086/588136](https://doi.org/10.1086/588136).
28. Pe'er A, Ryde F. Theoretical Implications of Thermal Emission from Gamma-Ray Bursts.
29. 2009, AIP Conference Proceedings, 1133, 317-322. [10.1063/1.3155909](https://doi.org/10.1063/1.3155909).
30. Peng Z. Y, Ma L, Zhao X H, Yin Y, Fang L M, Bao Y Y. The E_p Evolutionary Slope Within the Decay Phase of "Fast Rise and Exponential Decay" Gamma-Ray Burst Pulse. *The Astrophysical Journal*, 2009, 698, 417-427. [10.1088/0004-637X/698/1/417](https://doi.org/10.1088/0004-637X/698/1/417).
31. Rees M J, Mészáros P. Unsteady Outflow Models for Cosmological Gamma-Ray Bursts. *Astrophysical Journal Letters*, 1994, 430, L93-L96. [10.1086/187446](https://doi.org/10.1086/187446)
32. Rees M J, Mészáros, P. Dissipative Photosphere Models of Gamma-Ray Bursts and X-Ray Flashes. *The Astrophysical Journal*, 2005, 628, 847-852. [10.1086/430818](https://doi.org/10.1086/430818).
33. Rosswog S, Ramirez-Ruiz E, Davies M B. High-resolution calculations of merging neutron stars - III. Gamma-ray bursts. *Monthly Notices of the Royal Astronomical Society*, 2003, 345(4), 1077-1090. [10.1046/j.1365-2966.2003.07032.x](https://doi.org/10.1046/j.1365-2966.2003.07032.x)
34. Ryde F. The Cooling Behavior of Thermal Pulses in Gamma-Ray Bursts. *The Astrophysical Journal*, 2004, 614, 827-846. [10.1086/423782](https://doi.org/10.1086/423782).

35. Ryde F. Is Thermal Emission in Gamma-Ray Bursts Ubiquitous? *The Astrophysical Journal*, 2005, 625, L95-L98. [10.1086/431239](https://doi.org/10.1086/431239).
36. Ryde F, Pe'er A. Quasi-blackbody Component and Radiative Efficiency of the Prompt Emission of Gamma-ray Bursts. *The Astrophysical Journal*, 2009, 702, 1211-1229. [10.1088/0004-637X/702/2/1211](https://doi.org/10.1088/0004-637X/702/2/1211).
37. Sari R, Piran T, Narayan R. Spectra and Light Curves of Gamma-Ray Burst Afterglows. *The Astrophysical Journal*, 1998, 497, L17-L20. [10.1086/311269](https://doi.org/10.1086/311269).
38. Sironi L, Spitkovsky, A. Synthetic Spectra from Particle-In-Cell Simulations of Relativistic Collisionless Shocks. *The Astrophysical Journal*, 2009, 707, L92-L96. [10.1088/0004-637X/707/1/L92](https://doi.org/10.1088/0004-637X/707/1/L92).
39. Tavani M. A Shock Emission Model for Gamma-Ray Bursts. II. Spectral Properties. 1996, *The Astrophysical Journal*, 466, 768-778. [10.1086/177551](https://doi.org/10.1086/177551).
40. Woosley S. E. Gamma-Ray Bursts from Stellar Mass Accretion Disks around Black Holes. *The Astrophysical Journal*, 1993, 405, 273-277. [10.1086/172359](https://doi.org/10.1086/172359).
41. Yonetoku D, Murakami T, Nakamura T, Yamazaki R, Inoue A K, Ioka K. Gamma-Ray Burst Formation Rate Inferred from the Spectral Peak Energy-Peak Luminosity Relation. *The Astrophysical Journal*, 2004, 609, 935-951. [10.1086/421285](https://doi.org/10.1086/421285).
42. Yu H.-F, Preece R D, Greiner J, Narayana B P, Bissaldi E, Briggs M S, et al. The Fermi GBM gamma-ray burst time-resolved spectral catalog: brightest bursts in the first four years. *Astronomy & Astrophysics*, 2016, 588, 135-154. [10.1051/0004-6361/201527509](https://doi.org/10.1051/0004-6361/201527509).
43. Zhang B, Mészáros P. Gamma-Ray Bursts: progress, problems & prospects. *International Journal of Modern Physics A*, 2004, 19, 2385-2472. [10.1142/S0217751X0401746X](https://doi.org/10.1142/S0217751X0401746X).
44. Zhang B, Pe'er A. Evidence of an Initially Magnetically Dominated Outflow in GRB 080916C. *The Astrophysical Journal Letters*, 2009, 700, L65-L68. [10.1088/0004-637X/700/2/L65](https://doi.org/10.1088/0004-637X/700/2/L65).
45. Zhang B, Yan H. The Internal-collision-induced Magnetic Reconnection and Turbulence (ICMART) Model of Gamma-ray Bursts. *The Astrophysical Journal*, 2011, 726-752, 90. [10.1088/0004-637X/726/2/90](https://doi.org/10.1088/0004-637X/726/2/90).
46. Zhang B. Gamma-Ray Burst Prompt Emission. *International Journal of Modern Physics D*, 2014, 23, 1430002. [10.1142/S021827181430002X](https://doi.org/10.1142/S021827181430002X).